

UNCLASSIFIED

AD NUMBER

AD275366

LIMITATION CHANGES

TO:

Approved for public release; distribution is unlimited.

FROM:

Distribution authorized to U.S. Gov't. agencies and their contractors;  
Administrative/Operational Use; MAY 1962. Other requests shall be referred to Air Force Arnold Engineering Development Center, Arnold AFB, TN.

AUTHORITY

aedc usae ltr 15 oct 1968

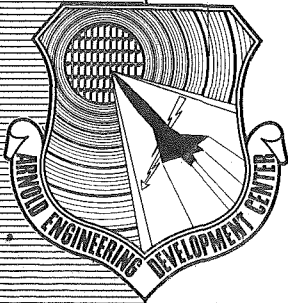
THIS PAGE IS UNCLASSIFIED

AEDC-TDR-62-78

C#1

cy1

**ARCHIVE COPY  
DO NOT LOAN**



**THE EFFECT OF HEAT RELEASE  
ON THE FLOW PARAMETERS  
IN SHOCK-INDUCED COMBUSTION**

By

**R. P. Rhodes, P. M. Rubins, and D. E. Chriss**

**Rocket Test Facility  
ARO, Inc.,  
a subsidiary of Sverdrup and Parcel, Inc.**

**TECHNICAL DOCUMENTARY REPORT NO. AEDC-TDR-62-78**

**May 1962**

**TECHNICAL REPORTS  
FILE COPY**

PROPERTY OF U. S. AIR FORCE  
AEDC LIBRARY  
AF-40(600)-800

**AFSC Program Area 801A, Projects 9751 & 6952, Tasks 37510 & 695201**

(Prepared under Contract No. AF 40(600)-800 S/A 24(61-73) by ARO, Inc.,  
contract operator of AEDC, Arnold Air Force Station, Tennessee)

PROPERTY OF U. S. AIR FORCE  
AEDC TECHNICAL LIBRARY

**ARNOLD ENGINEERING DEVELOPMENT CENTER  
AIR FORCE SYSTEMS COMMAND  
UNITED STATES AIR FORCE**

AEDC TECHNICAL LIBRARY



This document has been approved for public release  
its distribution is unlimited. Doc# AEDC-711

# NOTICES

Qualified requesters may obtain copies of this report from ASTIA. Orders will be expedited if placed through the librarian or other staff member designated to request and receive documents from ASTIA.

When Government drawings, specifications or other data are used for any purpose other than in connection with a definitely related Government procurement operation, the United States Government thereby incurs no responsibility nor any obligation whatsoever; and the fact that the Government may have formulated, furnished, or in any way supplied the said drawings, specifications, or other data, is not to be regarded by implication or otherwise as in any manner licensing the holder or any other person or corporation, or conveying any rights or permission to manufacture, use, or sell any patented invention that may in any way be related thereto.

~~ASTIA RELEASE TO OTS IS~~  
~~NOT AUTHORIZED~~

This document has been approved for public release and sale; its distribution is unlimited.

*per AF letter, 15 Oct. 68, signed William O. Cole*

THE EFFECT OF HEAT RELEASE  
ON THE FLOW PARAMETERS  
IN SHOCK-INDUCED COMBUSTION

By

R. P. Rhodes, P. M. Rubins, and D. E. Chriss

Rocket Test Facility

ARO, Inc.,

a subsidiary of Sverdrup and Parcel, Inc.

May 1962

ARO Project No. 150067



## **FOREWORD**

This project was partially funded by the Air Force Office of Scientific Research under AFOSR Project 9751 Task 37510.

## ABSTRACT

Experimental investigations were conducted in a Mach 3 combustion tunnel to determine heat release characteristics of a hydrogen-air mixture after it had passed through a normal shock. Inlet temperature was varied from 1800 to 3000°R. Heat release was indicated by three types of measurements:

1. Combustion and total temperature rise calculated from gas analysis
2. Total pressure loss caused by heat addition
3. Ultra-violet emission at the OH emission frequencies, indicating an  $H_2-O_2$  reaction

Combustion efficiency was found to increase with temperature and to be independent of fuel-air ratio.

Fuel passing through an oblique shock was observed to emit a radiation similar to that observed from the normal shock combustion.



## CONTENTS

	<u>Page</u>
ABSTRACT . . . . .	v
NOMENCLATURE . . . . .	xi
1.0 INTRODUCTION . . . . .	1
2.0 APPARATUS AND PROCEDURE	
2.1 Supersonic Combustion Tunnel . . . . .	2
2.2 Test Fuel Injection . . . . .	2
2.3 Wedges . . . . .	2
2.4 Instrumentation . . . . .	3
2.5 Data Reduction . . . . .	4
3.0 RESULTS AND DISCUSSION	
3.1 Flow Field Description . . . . .	5
3.2 Fuel Distribution . . . . .	9
3.3 Combustion Effects . . . . .	9
4.0 CONCLUDING REMARKS. . . . .	17
REFERENCES . . . . .	18
APPENDIXES	
A. Calculation Procedures . . . . .	21
B. Analysis of Chemical Reaction Quench Rates in the Gas Sampling Probe . . . . .	29

## ILLUSTRATIONS

Figure

1. Supersonic Combustion Tunnel with Normal Shock Configuration . . . . .	33
2. Schematic of Nozzle and Test Section Showing Normal Shock Configuration with Schlieren Photo of Shock System . . . . .	34
3. Fuel Injection Wedge . . . . .	35
4. Single Wedge Used to Produce Oblique Shock Waves . . . . .	36
5. Pressure and Sampling Probe . . . . .	37
6. Schematic of Pressure and Gas Sampling Equipment . . . . .	38
7. Mach Reflected Normal Shock Wave . . . . .	39
8. Variation of Flow Parameters on Tunnel Centerline . . . . .	40

<u>Figure</u>	<u>Page</u>
9. Effect of Preheater Temperature on Flow Parameters on Tunnel Centerline . . . . .	41
10. Total Pressure Profile Aft of Normal Shock Wave . . . . .	42
11. Total Temperature Traverse - No Test Fuel	
a. Horizontal . . . . .	43
b. Vertical . . . . .	44
c. Axial . . . . .	45
12. Preheater Gas Composition vs Total Temperature. .	46
13. Preheater Gas Properties vs Total Temperature . .	47
14. Fuel Distribution as a Function of $T_{t_0}$ . . . . .	48
15. Variation of Combustion Parameters across the Tunnel Width	
a. Low Inlet Temperature Level . . . . .	49
b. Medium Inlet Temperature Level. . . . .	50
c. High Inlet Temperature . . . . .	51
16. Combustion Efficiency as a Function of Inlet Temperature . . . . .	52
17. Variation of Flow Parameters on Centerline with Test Fuel Combustion . . . . .	53
18. Variation of Combustion Efficiency with Residue Time Aft of the Normal Shock . . . . .	54
19. Correlation of a Global Rate Equation for the Hydrogen-Oxygen Reaction . . . . .	55
20. Total Pressure Loss vs Fuel Concentration with Near-Zero Heat Release . . . . .	56
21. Total Pressure Loss vs Fuel Concentration at Various Combustion Efficiency Values . . . . .	57
22. Corrected Total Pressure Loss vs Temperature Ratio Three Inches Aft of the Normal Shock . . . . .	58
23. Variation of Flow Parameters with Axial Distance Aft of Normal Shock Wave with Test Fuel. . . . .	59
24. Comparison of Calculated Pressure Loss with Experimental Pressure Loss for Heat Addition Aft of the Normal Shock	
a. $T_{t_0}$ at shock 2750°R . . . . .	60
b. $T_{t_0}$ at shock 2350°R . . . . .	61

<u>Figure</u>	<u>Page</u>
25. Test Section Schlieren and Emission Photograph with Test Fuel On . . . . .	62
26. Test Section Emission Photograph with Test Fuel Off . . . . .	63
27. Test Section Emission Photograph with Oblique Shock Wave . . . . .	64



## NOMENCLATURE

$a_t$	Speed of sound at total temperature, ft/sec
$a_2$	Excess fuel over stoichiometric equivalence ratio
$E$	Global activation energy, cal/gm mole
$g$	Dimensional constant, $\text{lb}_m \text{ ft} / \text{lb}_f \text{ sec}^2$
$h$	Enthalpy, Btu/ $\text{lb}_m$ mole
$M$	Mach number
$m$	Molecular weight
$m_i$	Mole fraction
$p$	Pressure, psia
$Pr_t$	Turbulent Prandtl number
$p_t$	Total pressure behind a normal shock, psia
$p_{t_0}$	Plenum pressure, psia
$Q_r$	Heat of reaction, Btu/ $\text{lb}_m$ mole
$R_0$	Universal gas constant, energy/ $\text{lb}_m$ mole $^{\circ}\text{R}$
$T$	Temperature, $^{\circ}\text{R}$
$T_{t_0}$	Total temperature with $\epsilon = 0$ , $^{\circ}\text{R}$
$V$	Velocity, ft/sec
$X$	Axial distance behind shock wave, in.
$Y$	Vertical distance from tunnel centerline, in.
$y_1$	Preheater fuel concentration in equivalence ratio
$y_2$	Test fuel concentration in equivalence ratio
$Z$	Horizontal distance from tunnel centerline, in.
$\gamma$	Specific heat ratio
$\epsilon$	Combustion efficiency of test fuel
$\eta$	Overall combustion efficiency, test fuel and preheater fuel
$\rho$	Density, $\text{lb}_m / \text{ft}^3$
$\tau$	Time, microsec
$[A]$	Moles of component A per unit volume



(A) Volumetric fraction of component A in mixture (dry)

**SUBSCRIPTS**

c	Centerline
f	Test fuel only
p	Preheater only
pf	Preheater and test fuel
t	Total
1	Initial conditions
2	Final conditions
$\infty$	Free stream

## 1.0 INTRODUCTION

Although the chemical reaction rate of hydrogen has been studied for many years, little information is available on the effect of the aerothermodynamics of a supersonic airstream on the chemical reaction rate. Many theoretical analyses of devices using supersonic combustion have been made - for example ramjet engines (Refs. 1, 2, and 3). However, the problem of how this combustion can be stabilized and controlled has not been solved.

Although detonations in shock tubes have been studied previously, the attempt to work with "standing" waves is relatively recent. Nicholls (Refs. 4 and 5) used a normal shock wave produced by a highly under-expanded free jet nozzle. Gross (Ref. 6) and Rhodes and Chriss (Ref. 7) used a normal shock produced by the intersection of two wedge shocks.

This report discusses the work done in the Rocket Test Facility (RTF), Arnold Engineering Development Center (AEDC), Air Force Systems Command (AFSC), using the Supersonic Combustion Tunnel (SCT) as a continuation of the work reported in Ref. 7. Extensive data are presented on the flow field characteristics in the zone of the two-wedge shock and on the chemical reaction rate of hydrogen-air mixtures in this flow field when the temperature level is high enough for chemical action to occur. The work was directed toward establishing a simple aerodynamic model in which combustion phenomena could be studied with uncomplicated instrumentation which could measure conditions at a point in the stream. In these experiments, the objective was to verify whether heat release actually occurred, and, if so, to what extent. This was done by:

1. Sampling combustion gases through a probe specially designed to promote rapid quench of the chemical reactions and determining total temperature and other properties of the gas from an analysis of the gas composition;
2. Making extensive pressure surveys and comparing the measurements to those predicted by theoretical equations to determine whether deviations were caused by heat release; and
3. Measuring the radiant emission from the reaction with a spectrometer to determine whether radiation was caused by OH ion emission, and hence that an  $H_2 - O_2$  reaction was in progress.

Ultimately, knowledge gathered from these studies could be useful in the design of high-speed propulsion systems.

## 2.0 APPARATUS AND PROCEDURE

### 2.1 SUPERSONIC COMBUSTION TUNNEL

A detailed description of the Supersonic Combustion Tunnel (Fig. 1) is presented in Ref. 7. Air, preheated by an indirect-fired heater to  $1460^{\circ}\text{R}$ , enters the plenum where the core of the nozzle airflow is further heated to a maximum of  $3500^{\circ}\text{R}$  by the combustion of hydrogen. The nozzle is two-dimensional and initially had an exit area 3 in. wide by 5 in. high. It is operated as a free jet with a discharge Mach number of 3.1 inside the test rhombus.

During these tests the tunnel width was increased to six inches. This did not seem to have any effect on the flow parameters except to widen the zone in the center which was free of disturbances from the sidewalls.

The procedure for establishing the desired conditions in the test section is described in detail in Ref. 7.

### 2.2 TEST FUEL INJECTION

A decision was made early in the program to use a thin wedge fuel injector installed in the supersonic zone of the nozzle (Figs. 1 and 2), rather than the tube fuel injector near the tunnel throat used in the tests reported in Ref. 7. The purpose of this modification was to reduce the possibility of partial burning of fuel near the injector where the static temperature was quite high. Some experiments with throat fuel injection at the higher temperatures indicated that this type of partial burning was occurring. A photograph of the fuel injector is shown in Fig. 3. Further analysis of the wedge aerodynamics will be found in section 3.1.1.

### 2.3 WEDGES

Two types of wedges were used to produce shock systems. The first was a single, water-cooled, 30-deg wedge for producing an oblique shock wave. This wedge was mounted in a window frame as shown in Fig. 4. The second type consisted of a set of two 25-deg wedges used to produce a pair of oblique shocks and a connecting normal shock. The shock system produced and the location of the wedges are shown in Fig. 2. The photograph in Fig. 1 shows the wedges retracted from the test position.

## 2.4 INSTRUMENTATION

All temperatures except the test section total temperature were measured with chromel-alumel thermocouples and recorded on a recording potentiometer. The total temperature in the test section was calculated using the analysis of the gas as shown in Appendix A.

All air pressures except the total and static pressures in the test section were measured with a 120-in., mercury-filled, manometer board and recorded photographically.

Hydrogen pressures were measured with transducers and recorded on a recording potentiometer.

A water-cooled probe was used alternately for obtaining gas samples and total pressure measurements in the test section. When required, a second probe was used to measure the static pressure. Figure 5 shows probes with and without the static tube. The total pressure and static pressure were recorded as a function of position (the Z tunnel coordinate) on an x-y plotter. A schematic diagram of the total pressure, static pressure, and gas sampling system is shown in Fig. 6.

Samples were pumped from the probe with a dry diaphragm pump which maintained a pressure of 2 to 3 psi inside the probe and delivered the samples to the analyzers at slightly above atmospheric pressure. A water separator and chemical drier were used in the sampling lines and all analyses were made on a dry basis. Local concentration of hydrogen in the test section was measured by a thermal conductivity meter described in Ref. 7. Local concentration of oxygen was measured by a meter which detects the change in the magnetic susceptibility of the gas. The oxygen meter was calibrated using nitrogen for a zero and atmospheric oxygen for 20.95-percent oxygen. The oxygen and hydrogen concentrations were recorded on a recording potentiometer. An analysis of the mechanism of sampling is discussed in Appendix B.

Shock position, axial and vertical position of the test section probe, and location of emission from high temperature zones were determined photographically. The test section was photographed with a schlieren camera using either collimated light from a spark source or direct emission from the test section. The schlieren spark was collimated to a 6-inch beam by an aerial camera lens. This light and the emission from the test section were focused on a 4 in. by 5 in. camera.

## 2.5 DATA REDUCTION

Pressure data were read from manometer board photographs or x - y recorder charts and reduced manually. Temperature and compositions were obtained from a computer solution of the equations given in Appendix A. An estimate of the accuracy of the raw and reduced data is also given in Appendix A.

## 3.0 RESULTS AND DISCUSSION

Shock-induced combustion occurs when a premixed combustible mixture is heated to above its ignition temperature by passing through a shock wave. The most familiar example of this is the classical detonation wave in which a constant area boundary condition is imposed on the flow. In this case the energy needed to drive the shock wave is supplied by the combustion. This is the type of phenomenon seen in a detonation tube. Here, the final conditions are determined by the initial conditions and the application of conservation of mass, momentum, and energy.

Previous workers with shock-induced combustion waves have assumed that the thermodynamics of constant area classical detonations are applicable to all shock-induced combustion waves (Refs. 4 and 7). It would seem, however, that other aerodynamic processes for releasing heat using shock-induced combustion would be possible if different boundary conditions are applied. It is possible to describe theoretically a constant pressure, shock-induced combustion wave where the gases heated by the combustion expand so that the static pressure in the combustion zone is the same as the static pressure behind the shock wave without combustion. Physically this might occur if a combustible core of gas passing through a shock wave had a relatively small diameter compared to the reaction zone length so that the expansion of the heated gases would not appreciably change the static pressure behind the shock wave. It might also occur in a variable area duct where the contour exactly matched the rate of heat addition to maintain constant static pressure. As long as the rate of expansion caused by heat addition is low compared to the velocity of the burning gas, there will be negligible radial pressure gradients across the combustion zone; and, if a step profile can be assumed, a one-dimensional flow approximation will describe the flow. As the ratio of the diameter to the length of the reaction zone increases, the pressure at the center of the reaction zone approaches the constant area value because three-dimensional expansion will cause sizeable pressure gradients from the center to the outside of the combustion zone. Constant pressure shock-induced combustion is then limited to combustion zones with long enough reaction times and slow enough expansion so that these three-dimensional effects are negligible. This type of reaction

cannot produce a normal shock wave ahead of it because the same size and reaction rate criteria which allowed the one-dimensional approximation will preclude the pressure rise necessary to produce the shock wave. Again the terminal conditions of the constant pressure case can be determined explicitly from the inlet conditions and the continuity equations.

A more complicated case arises when there is an axial static pressure gradient behind the shock wave. For a small diameter combustion zone, this pressure can exist independent of the combustion. If the combustion zone size and the reaction rate are small enough and step profiles are assumed, a one-dimensional approximation will in this case adequately define the flow; however, the final conditions will depend on the velocity at which the heat is added as well as on the inlet conditions. The terminal conditions are not defined by the inlet conditions and the total heat release as they are in the other cases mentioned. In this case the static temperature and therefore the rate of the reaction will be influenced by the pressure gradient.

The last case is the model which was used for the analysis of the data from the SCT. A static pressure gradient exists behind the shock system which depends on the interaction of the shock and expansion waves. The assumption that this pressure gradient is independent of combustion was verified by the data. Total pressure loss for a given amount of heat release depends on the location in this pressure field where the heat is released.

All the possible boundary conditions are not limited to those mentioned thus far, since by application of the proper pressure gradient or area change it would be theoretically possible to achieve heat release at constant Mach number or constant static temperature, although these might be impossible to achieve in practice. In an actual combustion system, combinations of diffusional and shock-induced combustion may exist, and one-dimensional theory would not be adequate. This system would be even more difficult to analyze, although over-all performance may be measurable.

### 3.1 FLOW FIELD DESCRIPTION

In this section are described the aerodynamic and thermal conditions which exist in the test section of the SCT which establish the boundary conditions for the combustion. This information is based on total pressure and total temperature traverses and on a limited amount of static pressure data.

A general schematic of a Mach reflected normal shock system is shown in Fig. 7. The "normal"-shock wave is produced because the turning angle necessary to straighten the flow behind the first oblique shock is greater than the maximum turning angle at this Mach number, so that a simple reflection cannot occur. The flow at the shock intersection is not turned parallel and contracts with supersonic flow outside and subsonic flow inside the slip line. Mixing occurs along this boundary resulting in the reacceleration of the center flow both by contraction of the flow and by the mixing with higher energy air.

The configuration used for the normal shock studies has been described in the section on apparatus and shown, with the shock system produced by this configuration, in Fig. 2.

### 3.1.1 Pressure Effects Ahead of the Normal Shock Wave

In the region ahead of the normal shock wave the air accelerates nearly isentropically from the throat until it passes around the fuel injection wedge which causes a reduction in total pressure. As a result of wedge interference, the total pressure and Mach number profiles of the air approaching the normal shock wave are distorted and have minimum values at the tunnel horizontal centerline (Fig. 7).

A calculation was made to determine if the discrepancy between the indicated total pressures measured at the centerline and the theoretical value for a Mach 3.1 normal shock wave could be explained. The pressure loss caused by the fuel injection wedge was compared to the momentum per unit area at the shock wave with the inlet momentum minus the wedge drag. It was assumed that the dimensionless velocity ratio  $(V - V_{\infty}/V_c - V_{\infty})^{P_{t0}}$  resulting from the wedge drag without fuel injection is the same as the dimensionless concentration profile  $(y/y_c)$  when there was fuel injected (Ref. 8). A turbulent Prandtl number of 0.5 was assumed. Constant static pressure was assumed along the mixing zone.

The momentum at the shock wave was  $1/p \int \rho V^2 dV$  per square inch where

$$\frac{\rho V^2}{p} = \gamma (V/a_t)^2 \left[ 1 - \frac{\gamma - 1}{2} (V/a_t)^2 \right]^{-1} \quad (\text{Ref. 10})$$

and since for a given test condition  $a_t$  was constant

$$(V/a_t)_{at \ y} = (V_c/a_t - V_{\infty}/a_t) (y/y_c)_{at \ y}^2 + V_{\infty}/a_t$$

where  $V_c/a_t$  was calculated from  $\frac{P_{t0}}{P_{t0}}$  (experimental) and  $\frac{P}{P_{t0}}$  (isen,  $M = 3.1$ );

$V_{\infty}/a_t$  was calculated for isentropic  $M = 3.1$ ; and  $(y/y_c)$  was the fuel distribution at the same total temperature.

The momentum at the fuel injector was assumed to be the momentum calculated from isentropic relationships at  $M = 3.1$  minus the wave drag and skin drag on the wedge.

The following table compares the momentum at the wedge with that at the shock for two total temperatures.

<u><math>T_t - ^\circ R</math></u>	<u><math>\rho V^2/p</math></u>	
	<u>At the Wedge</u>	<u>At the Shock Wave</u>
1500	12.66	12.54
2750	12.11	12.17

The agreement between the momentum calculated at the two stations is close enough that the reduction in total pressure over that expected for a Mach 3.1 normal shock wave can be explained by the momentum loss on the fuel injection wedge.

### 3.1.2 Pressure Effects Aft of the Normal Shock Wave

Several pressure profiles were taken in the region behind the normal shock wave with the preheater on but without test fuel injection. Figure 8 shows the data from an axial static pressure and a pitot total pressure traverse. The static pressure at the shock wave was calculated from the theoretical normal shock static pressure rise at the centerline; based on the measured indicated total pressure and the isentropic static pressure at a free-stream Mach number of 3.1, the static pressure falls rapidly from the shock wave aft and the indicated total pressure falls more slowly.

As may be seen from the data (Fig. 8), the static pressure is almost independent of total temperature. This is not true for the total pressure. As the total temperature is increased, the indicated total pressure ratio increases (Fig. 9). This increase results from a greater spreading of the wake from the fuel injection wedge at higher temperatures [see fuel distributions (Fig. 14)] which spreads the wedge loss over a greater area and reduces the maximum loss.

Pressure profiles taken in the vertical and horizontal direction resulted in curves of the type seen in Fig. 10. The horizontal profiles are nearly flat in the center. The vertical profiles are strongly curved indicating both the disturbance from the wedge and the transition in Mach number as the probe crosses the slip lines from the shock intersection.



From the static and indicated total pressure data, the centerline Mach number and total pressure may be calculated. These parameters are plotted in Figs. 8 and 9. The Mach number increases from the normal shock value just behind the shock wave to a supersonic value at less than three inches downstream of the shock wave (Fig. 8). The Mach number at three inches aft also increases with an increase in total temperature (Fig. 9).

In SCT when a combustible mixture is heated by passing through the normal shock wave, it immediately enters a flow field where the velocity is increasing and the static temperature is decreasing. Therefore, any pressure losses from combustion will depend greatly on the axial position at which the combustion occurs. Also, the static temperature drop from the flow acceleration will affect the temperature rise from combustion and may greatly change the course of the reaction.

### 3.1.3 Total Temperature Profiles

Total temperature profiles were made at various locations in the test section. The temperatures were determined from the analysis of the combustion gases from the hydrogen-fired preheater using 100-percent combustion efficiency (see Procedure). No free hydrogen was ever detected in the test section unless test fuel was being introduced. Typical temperature profiles may be seen in Fig. 11. The profiles are relatively flat over the area of interest at any given axial station. There is, however, a gradual axial drop in temperature toward the rear which results from mixing of the heated core with surrounding cooler air.

As the total temperature is increased, the oxygen content of the air decreases and the water vapor increases. Figure 12 shows the ideal relationship between the total temperature and the gas composition. This produces an added complication since the physical and chemical properties of the preheater gases are a very complicated function of temperature. Figure 13 shows how some of the more useful of these properties vary.

For the preheater gases without test fuel,  $T_{t_0}$  is the total temperature at the sampling point. When test fuel is added,  $T_{t_0}$  is the total temperature of the mixture with  $\epsilon = 0$ .  $T_t$  is the final temperature of the combustion products at the same location.

The addition of cold test fuel changes the temperature and composition still further. This effect will be discussed in the section on combustion efficiency.

### 3.2 FUEL DISTRIBUTION

Fuel injected from a small hole in the downstream side of the fuel injector wedge (Fig. 3) proceeds downstream. While traveling, it mixes with the surrounding air. The rate of mixing is influenced by difference in velocity between fuel and air and by temperature levels. After traveling about six inches in a Mach 3 flow, the mixture passes through a shock where reaction may or may not occur depending on the gas temperature.

Fuel concentration was calculated from analysis of oxygen and hydrogen content by the method described in Appendix A. Data with test fuel combustion will give the hydrogen equivalence ratio ( $y_1 + y_2 + a_2$ ). Since the same preheater level without test fuel will give  $y_1$ , the test fuel will be the difference of the two calculated equivalence ratios. The resulting fuel concentration profiles were plotted in Fig. 14 and closely resemble a normal distribution curve of the form  $K(e)^{-bZ^2}$ , where  $K$  and  $b$  are coefficients and  $Z$  is a tunnel coordinate distance perpendicular to the flow in the horizontal plane. Figure 14 shows a marked increase in rate of mixing of the fuel as preheater temperature is increased. A comparison of fuel profile peaks at the fore and aft position in Fig. 14 also shows a decrease in fuel concentration with distance from the normal shock.

### 3.3 COMBUSTION EFFECTS

One of the primary purposes of these experiments was to show that heat release actually occurred in the area aft of the shock, and, if possible, to what extent. This was investigated by three methods; temperature measurements, pressure measurements, and radiation emission. They will be discussed separately.

#### 3.3.1 Effect of Temperature on Combustion

One of the overall objectives of this study was to determine the rate of reaction of hydrogen-air mixtures. As an initial part of this investigation, the combustion efficiency was measured at various locations in the combustion zone. These data are correlated with position relative to the shock wave and with the inlet temperature. An attempt was also made to determine a reaction rate as a function of the combustion mixture temperature.

**3.3.1.1 Combustion Efficiency.** The combustion efficiency,  $\epsilon$ , is defined in this report as the ratio of the test fuel burned to the total test

fuel present that could burn. As was previously mentioned the preheater operates at 100-percent combustion efficiency, and the preheater hydrogen is not counted in calculating the test fuel combustion efficiency.

Accuracy with which the efficiency and temperature can be measured depends on two factors: (1) the accuracy with which the composition of the sampled gas can be determined (see Appendix A) and (2) the rate at which the reaction is quenched as it enters the probe. The rate of quench is discussed in greater length in Appendix B. However, it should be noted that free radical recombinations cannot be quenched; that is, any OH, H, or O will recombine to form  $H_2O$ ,  $H_2$ , and  $O_2$ . Any energy released during these recombinations will increase the temperature of the gas after it has entered the probe. The recombinations can be ignored if the efficiency is considered as the hydrogen consumed. Calculated temperatures and energy release will be higher than the free-stream values by the dissociation energy of the free radicals present, even if it is assumed that the dissociation and branching reactions are completely quenched.

The relationship between  $\epsilon$  three inches downstream of the normal shock and total temperature ( $T_{t_0}$ ) is shown in Fig. 15. Figures 15a, b, and c show how  $\epsilon$  varies along the horizontal centerline for several inlet temperatures. The gas temperature from the preheater is nearly uniform along the horizontal centerline when no test fuel is added; but in calculating a correction for the cold test fuel it was found that there is a reduction in total temperature which is proportional to the total test fuel added. Figure 16 shows  $\epsilon$  as a function of total temperature ( $T_{t_0}$ ) corrected for the cooling effect of the hydrogen at an axial position three inches aft of the normal shock wave. At this station for a plenum total pressure of 50 psia the efficiency is, within the experimental error, a function of inlet total temperature only, with no noticeable effect of fuel concentration. The static temperature of the gas just behind the shock wave may be calculated by multiplying  $T_{t_0}$ , corrected for the total temperature rise along the axis (Fig. 11c), by the static to total temperature ratio at the shock wave (From M in Fig. 8). A resulting inlet static temperature of about 2300°R is required to produce 50-percent combustion efficiency in three inches and about 1950°R to produce five-percent combustion in the same distance.

In a system such as this where the flow accelerates rapidly behind the shock wave, the combustion efficiency rises rapidly at first, and then as the static temperature reaches a maximum, its rate of rise decreases (Fig. 17). The static temperature rises rapidly at first because the total temperature is increasing. However, at the same time the static to total temperature ratio is decreasing because of the flow acceleration. As the

reaction nears completion this effect becomes predominant, and the static temperature begins to decrease. Since the static temperature was calculated from Mach number and total temperature, the accuracy of this parameter depends on the accuracy of both the total temperature and the indicated static and total pressure measurements.

**3.3.1.2 Reaction Kinetics.** The relation between combustion efficiency and distance can be transformed to a relationship between combustion efficiency and time by calculating the velocity-distance relationship from experimental values of  $P_s$ ,  $P_t$ , and  $T_t$  and graphically integrating  $1/V$  vs  $X$  where  $\int_0^X 1/V dX = \tau(X)$ . Figure 18 shows the  $\epsilon$  plotted as a function of  $\tau$ . The slope of this curve is  $d\epsilon/d\tau$  which equals  $-\frac{1}{(H_2)_t} \frac{d(H_2)}{d\tau}$ . A global equation for the rate of consumption of hydrogen can be written as:

$$-\frac{d[H_2]}{dt} = [H_2]^n [O_2]^m A e^{-\frac{E}{R_o T}}$$

where  $A$  is a constant,  $E$  is the global activation energy, and  $m$  and  $n$  are constants which determine the overall order of the reaction.

If the proper values for  $m$  and  $n$  are known and one relationship will describe the whole reaction, a plot of  $\log A e^{E/R_o T}$  vs  $1/T$  will be a straight line, where the slope is  $E/R_o$  and the intercept at  $E/R_o T = 1$  is  $A$  (Fig. 19). The data shown in this figure came from two runs at different inlet temperatures. The activation energies, as represented by the slope of the curves, were calculated from the two sets of data and are nearly the same above a static temperature of 2800°R. The change in slope below 2800°R could result because the global equation, as written, does not describe the reaction over a broad temperature range or because of errors in the data at the lower temperature. The difference in the intercepts of the two curves also shows that the equation does not describe the reaction completely. The calculated activation energy is close to that for the reaction  $H_2 + O \longrightarrow OH + H$  which has been proposed as the rate controlling step in the hydrogen-oxygen combustion (Ref. 4). However, there are an insufficient number of data points to establish a definite value for the constants in a global equation.

Between 0.5 in. and 3 in. aft of the shock wave, the change in combustion efficiency is very small (Fig. 17). Reaction rates in this range are much lower and do not fit the same global equation as they do in the early part of the reaction. It is possible that the rate of change of hydrogen concentration is affected by mixing or that an apparent change results from a failure of the probe to follow a streamline.

### 3.3.2 Effect of Temperature Rise on Total Pressure

As a further attempt to verify heat release, total pressure was measured at various inlet total temperature levels and locations in the zone of interest downstream of the normal shock, both with and without test fuel. Also, a simplified theoretical correlation of this data was attempted. For the case of no friction, mass addition, or molecular weight change (Ref. 6), the following relation may be written between total pressure and total temperature

$$\frac{dp_t}{p_t} = \frac{\gamma M^2}{2} \frac{dT_t}{T_t} \quad (1)$$

which, when integrated for the condition of constant Mach number and  $\gamma$ , becomes

$$\frac{p_{t_2}}{p_{t_1}} = \left[ \frac{T_{t_1}}{T_{t_2}} \right]^{\frac{\gamma M^2}{2}} \quad (2)$$

Although total pressure ratio is a function not only of total temperature ratio, but also of Mach number and  $\gamma$ , Eq. (2) may be used for a practical case where total temperature increases are small, and  $\gamma$ , Mach number, mass, and molecular weight changes may be considered to be insignificant. With this equation in mind, the data on pressure measurement will be examined.

First, Fig. 15 shows there are two pressure profile curves for each inlet gas temperature level ( $T_{t_0}$ ), one for the condition of preheater only and the other for preheater plus test fuel. Note also that the difference between the two curves increases with increased inlet temperature level. Here a total pressure loss is apparent when combustion occurs; however, total pressure loss may result from reduced molecular weight also.

Then in Fig. 20, the total pressure drop caused by unburned fuel is shown, and in Fig. 21 the effect of combustion is demonstrated by adding in a large group of data at various degrees of reaction completion. Now a family of lines can be drawn, showing the relation between heat release, fuel concentration, and total pressure loss. If the effect of pressure drop caused by unburned fuel is removed by using the data of Fig. 20, the curve of Fig. 22 may be drawn.

Thus far, only experimental data have been discussed, and it can be seen that the scattering of these results are well within the estimated experimental accuracy, as defined in Appendix A. In calculating the points for these curves, it was necessary to use total and static pressure measurements and total temperature,  $\gamma$ , and molecular weight from the gas analysis.

Now, the question arises, can the measurement of total pressure only be used to predict the quantity of heat release. The answer is no because enough additional information must be known to describe the properties of the flowing gas, such as Mach number,  $\gamma$ , and molecular weight. However, enough experimental information was obtained so that the pressure drop caused by heat addition could be separated from that caused by fuel, and with what is considered good agreement.

Equation (2) was used with a stepwise calculation. Temperature increments of 100°R were used. The initial Mach number conditions were calculated just aft of the normal shock, based on the plenum and test section pressures, analysis of the wedge effect on the flow (Section 3.1.1), and the fuel concentration. The axial static pressure profile was experimentally found to be independent of heat release at distances greater than one inch aft of the normal shock wave. Just behind the shock wave the static pressure was calculated from the free-stream static pressure at Mach 3.1 and the measured total pressure. Using this value and the experimental data, the pressure distribution curve of Fig. 23 is shown. The specific heat ratio ( $\gamma$ ) was calculated from the gas analysis and temperature determined from the gas analysis. Thus, an incremental total pressure drop was calculated, resulting in a new total pressure for the next increment. In this manner, the calculation was continued until the temperature rise tapered off to zero at a distance about 0.6 in. downstream of the shock. A comparison between the calculated total pressure loss and the experimental data, for the condition of test fuel injected and preheater on, is given in Fig. 24 at two different inlet temperatures. This correlation is considered good because a Mach number error of 0.05 used in the stepwise calculation would result in an error of about 0.2 percent per step and an overall error of about 3 percent. The uncertainties in the static pressure measurement could easily cause this difference.

These experimental pressure data were corrected for unburned fuel. It was assumed that the difference between the fuel-on and fuel-off total pressure just aft of the normal shock ( $X = 0$ ) was caused by the presence of unburned fuel, and that as the fuel burned, this effect was reduced proportionally to the concentration of fuel. Although water vapor was present, its overall effect was small compared to that of hydrogen, and therefore it was neglected. The resulting equations are:

$$\left[ \frac{\left( \frac{p_t'}{p_{t_o}} \right)_p - \left( \frac{p_t'}{p_{t_o}} \right)_{pf}}{\left( \frac{p_t'}{p_{t_o}} \right)_p} \right]_{X=0} = \begin{array}{l} \text{Pressure loss ratio caused by fuel} \\ \text{just aft of the normal shock} \end{array} \quad (3)$$

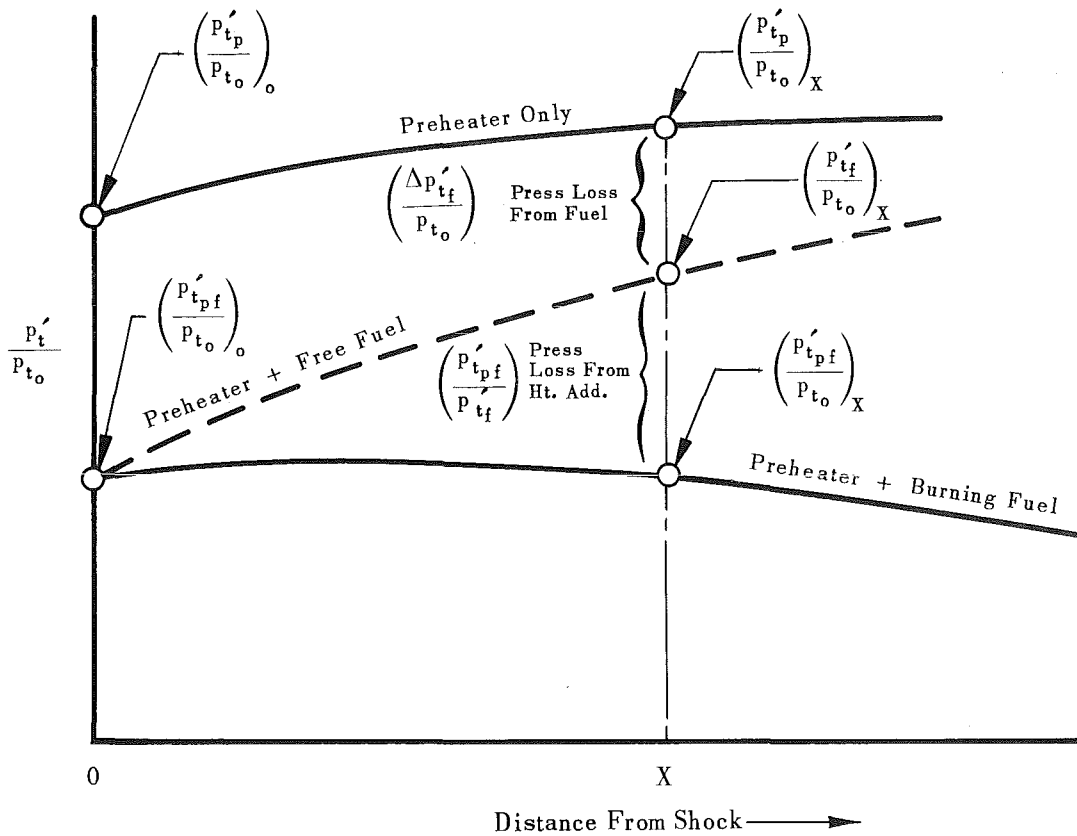
and

$$\frac{[(y_2 + a_2) - y_2 \epsilon]_X}{(y_2 + a_2)_0} \left[ \frac{\left(\frac{p'_t}{p_{t0}}\right)_p - \left(\frac{p'_t}{p_{t0}}\right)_{pf}}{\left(\frac{p'_t}{p_{t0}}\right)_p} \right]_0 = \left[ \frac{\Delta p'_{tf}}{p'_{tp}} \right]_X \quad (4)$$

so that

$$\left[ \frac{p'_{tpf}}{p'_{tf}} \right]_{\text{heat add. only}} = \frac{\left[ \frac{p'_{tpf}}{p'_{tp}} \right]_{\text{meas}}}{1 - \left[ \frac{\Delta p'_{tf}}{p'_{tp}} \right]_X} \quad (5)$$

The terms in the preceding equations are located on the following schematic diagram:



The correlation was calculated only to about 0.6 in. aft of the normal shock since (1) most of the temperature rise occurs within this distance and

(2) it was surmised that mixing losses were becoming pronounced at this point, which would have made further calculations irrelevant since the equations used did not account for mixing.

From the foregoing data and analysis, these conclusions may be stated:

1. There is a well defined pressure loss effect that can be attributed to (1) fuel injection losses when hydrogen is added and to (2) heat addition from combustion.
2. This effect may be correlated with simple theory, even though the flow field is changing, if sufficient information on the flow field is at hand.

### 3.3.3 Test Section Emission

During the investigation of hydrogen combustion initiated by a shock wave, pronounced emission was visible in the region behind the shock wave.

3.3.3.1 Normal Shock Wave. An emission photograph downstream of a normal shock wave was superimposed on a schlieren photograph and is shown in Fig. 25. This type of emission has been used to calculate an ignition delay time (Refs. 1, 2, and 4). However, in the SCT, although emission from the test section begins at an inlet total temperature of about 1700°R, the combustion efficiency does not exceed five percent unless the total temperature is above 2000°R.

In an attempt to determine the source of this radiation, a spectrogram (covering a wavelength from about 3000 to 6000 Å) was taken of the brightest part of the emission zone. A quartz prism spectrophotometer with a photomultiplier detector was used.

The only radiation which could be detected was emitted around 3050 Å which corresponds to the band head of the 0, 0 OH band at 3064 Å, and continuous radiation which, when analyzed, had the spectral distribution of a black body at 3400°R. The most logical explanation for the continuous radiation is that it comes from particulate matter in the stream. This is not to say that the particles are at 3400°R, since the emissivity of small particles will vary with wavelength and the relationship between true temperature and apparent black body temperature is quite complicated. The particles apparently were heated by the hydrogen combustion, since at inlet total temperatures up to 2800°R there is no glow without hydrogen. Above 2800°R there is an overall glow in the test section which becomes brighter as the temperature is increased and which is brighter behind the shock waves



where the static temperature is higher (Fig. 26). The fact that the location where the emission brightens is coincidental with the location of the shock waves would imply that at least some of the particles are very small ( $\ll 1$  micron) since they must be heated appreciably in less than one microsecond. Any longer delay than this could be detected as a gap between the shock waves as shown by the schlieren system and the shock waves as outlined by the emission increase. Other particles must be substantially larger since there is emission ahead of the shock wave where the static temperature is about  $1000^{\circ}\text{R}$ , and the particles radiating here must have retained their heat from the preheater. Within the limits of knowledge of the temperatures of the particles, a particle size distribution from 10 to 0.1 micron would probably satisfy these conditions. Gas stream analysis has shown small quantities of iron and aluminum oxides to be present in the supply air. This contamination probably originates from scale in the pipe and from the aluminum oxide air drier and could account for the observed effect.

It is possible that the emission which is seen could result from surface reactions which heat the particles without appreciably changing the gas temperature or the composition of the bulk of the stream. It is not known whether particles heated by surface reactions would affect the overall rate of the reaction, but it is possible that these reactions could cause an increase in the concentration of free radicals which could change the rate of the branching reactions. Also later in the reaction, the particles could provide a surface for recombination reactions. Both of these effects would cause an increase in the overall rate of conversion of hydrogen and oxygen to water vapor.

3.3.3.2 Oblique Shock Wave. The emission seen behind the shock wave when a normal shock configuration was used was also seen with the oblique shock wave configuration. Figure 27 shows emission photographs of the test section at an inlet total temperature of over  $3000^{\circ}\text{R}$  with nitrogen and then with hydrogen flowing through the fuel injector. Both photographs were processed in the same manner and show the relative intensity and location of the emission from the hot preheater gases and from the hydrogen reaction. The calculated static temperature immediately behind the oblique wave is the same as that behind a normal shock wave with a total inlet temperature of about  $2300^{\circ}\text{R}$ . Under these conditions a reaction should proceed in the main body of the gas on the order of 40 percent of the hydrogen burned in the first inch behind the oblique shock wave. This conclusion is based on the effect of inlet temperature on combustion efficiency (Fig. 16) and on the spacial distribution of the combustion zone (Fig. 17).

Several attempts were made to determine if there were a Mach number change resulting from heat addition behind an oblique wave by looking

for wave angle increases on small wedges mounted in the emission zone. Results of the data were inconclusive because of (1) aerodynamic effects which prevented the shock waves from being straight and clear-cut and (2) reduced density at high temperature which reduced the visible shock wave intensity as seen in the schlieren system. No data on composition changes were obtained because the gas sampling system was not in use at the time.

#### 4.0 CONCLUDING REMARKS

A series of tests were conducted in the Supersonic Combustion Tunnel to determine the efficiency of the combustion in a shock-induced combustion wave, the effect of the combustible mixture temperature on the combustion efficiency, and the relationship between the total pressure loss and the amount of heat release.

An aerodynamic analysis of the Mach reflected normal shock system showed a static pressure gradient behind the normal shock wave which caused the flow to be re-accelerated to about Mach 1.6 three inches downstream of the normal wave. This pressure gradient was independent of total temperature level and was unaffected by the presence of combustion behind the shock wave.

Hydrogen for shock-induced combustion was introduced from the center of a wedge-shaped strut located in the supersonic flow about six inches upstream of the normal shock wave. The fuel spread so that the entire height of the normal shock wave contained a combustible mixture. This spreading increased further downstream and also increased as the total temperature was raised.

When test fuel was introduced, the combustion efficiency rose rapidly at first and then at a lower rate. The decrease in rate resulted from a reduction in the quantity of hydrogen available to burn and from the reduction in static temperature caused by the expansion of the gas. Three inches downstream of the shock wave the combustion efficiency was a function of inlet total temperature and independent of the initial hydrogen concentration within the experimental accuracy of the data. Initial combustion occurred at a total temperature of about 1800°R, increased to 50 percent at about 2300°R and to 90 percent at about 3000°R.

The effect of temperature rise on total pressure loss was measured for several conditions of inlet temperature ( $T_{t_0}$ ) and position downstream of the normal shock and was correlated with fuel concentration and combustion efficiency. In addition, a correlation of pressure loss and

temperature rise was obtained by calculating the pressure loss for an incremental temperature rise with a simplified equation and, using the known factors about the flow field, then comparing the resulting values with the experimental data. Correlation between the calculated and experimental values was shown in the region just aft of the normal shock where the temperature rise occurred.

Emission from the combustion zone was detected at inlet total temperatures as low as 1700°R and increased in brightness as the temperature was raised. Spectral analysis showed this emission to consist of some radiation about the wavelength of the OH band emission and continuous radiation which increased from short to long wavelengths. It is possible that the continuous emission came from particles of iron and aluminum oxides heated to incandescence by surface chemical reactions.

Tests were made with a single wedge in an attempt to get oblique shock-induced combustion. Emission was seen behind the shock wave, but since no chemical analysis of the gas was taken behind the shock wave no quantitative evidence of combustion was obtained.

#### REFERENCES

1. Jamison, R. R. "Hypersonic Air Breathing Engines." Bristol-Siddeley Engines, Ltd., Paper prepared for Colston Symposium, Bristol, 1959.
2. Weber, R. J. and MacKay, J. S. "An Analysis of Ram Jet Engines Using Supersonic Combustion." NACA TN 4386, September 1958.
3. Dugger, G. L. "A Future for Hypersonic Ramjets." Astronautics, April 1959.
4. Nicholls, J. A. "Stabilization of Gaseous Detonation Waves with Emphasis on the Ignition Time Delay Zone." AFOSR TN 60-442, June 1960.
5. Nicholls, J. A., et. al. "On Experimental and Theoretical Study of Stationary Gaseous Detonation Waves." AFOSR-1764, October 1961.
6. Gross, R. A. "Exploratory Studies of Combustion in Supersonic Flow." AFOSR TN 59-587, June 1959.
7. Rhodes, R. P. and Chriss, D. E. "A Preliminary Study of Stationary Shock-Induced Combustion with Hydrogen-Air Mixtures." AEDC-TN-61-36, July 1961.

8. "Turbulent Flows and Heat Transfer." Princeton University Press, 1959, pp. 170-172.
9. Shapiro, A. H. "Dynamics and Thermodynamics of Compressible Flow, Vol. I." Ronald Press, 1953.
10. Ames Research Staff. "Equations, Tables, and Charts for Compressible Fluid Flow." NACA Report 1135, 1953.
11. Lewis Laboratory Computing Staff. "Tables of Various Mach Number Functions from 1.28 to 1.38." NACA TN 3981, April 1957.
12. Thrasher, L. W. and Binder, R. C. "A Practical Application of Uncertain Calculations to Measured Data." ASME Paper No. 55-A-205, 1955.
13. Keenan, J. H. and Kaye, J. Gas Tables. John Wiley and Sons, 1948.
14. Handbook of Chemistry and Physics, 34th Edition. 1952, pp. 1613, Chemical Rubber Publishing Co.
15. German, R. C. and Bauer, R. C. "Effects of Diffuser Length on the Performance of Ejectors without Induced Flow." AEDC-TN-61-89, August 1961.



## APPENDIX A

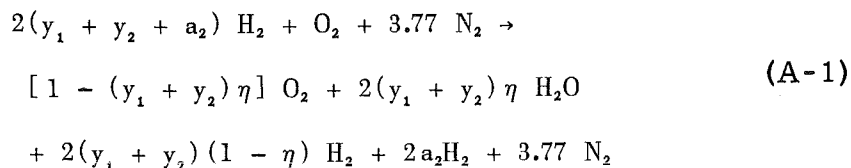
## CALCULATION PROCEDURES

## CHEMICAL REACTIONS

The chemical reactions of interest are located physically in two places: in the preheater where 1460°R air is heated to a higher temperature by combustion of hydrogen and in the test section where fuel is injected and reaction phenomena are observed.

Since all data to date indicate no residual hydrogen from the preheater reaction, combustion efficiency there was considered to be 100 percent. Combustion efficiency in the test zone is based on the ratio of fuel quantity that has disappeared in a reaction process as compared to the total fuel that could theoretically react. Hence, if the fuel concentration is greater than stoichiometric (equivalence ratio  $> 1$ ), the quantity of fuel in excess of stoichiometric is automatically excluded from the efficiency calculation. In order to accomplish this calculation, it was found necessary to calculate overall combustion efficiency of preheater and test fuel, insert the known value of preheater fuel concentration at 100 percent combustion efficiency, then calculate the resulting combustion efficiency of the test fuel.

The equilibrium reaction equation of H<sub>2</sub>-air after quenching and cooling, for various efficiencies, is as follows;



where  $\eta$  (overall combustion efficiency) is defined as:

$$\begin{aligned}
 \eta &= \frac{\text{amount of fuel burned}}{\text{amount of fuel that could be burned with available O}_2} \\
 \epsilon &= \text{combustion efficiency for test zone fuel} \\
 y_1 &= \text{equivalence ratio of fuel from preheater} \\
 y_2 &= \text{equivalence ratio of test fuel} \\
 a_2 &= \text{equivalence ratio of test fuel greater than E.R.} = 1.0
 \end{aligned}$$

The completely burned gas from the preheater may be analyzed and equivalence ratio (E.R.) calculated from Eq. (2) where  $H_2\% = 0$  and  $\eta = 100\%$ :

$$y_1 = \frac{1 - 4.77 (O_2)}{1 - O_2} \quad (A-2)$$

where

$(O_2)$  = percent of oxygen in the gas by volume,  
on a dry basis

Once  $y_1$  is established at a fixed preheater level, test fuel can be injected. Since test fuel can exist from 0 to 100 percent burned, both oxygen and hydrogen analyses are required to determine degree of the reaction completion. Here, it is assumed that the reaction is quenched a short interval of time after entering the sampling probe (see Appendix B), and that free radicals have recombined with their proper associates during the cooling process. With these assumptions, the following equation may be obtained from Eq. (A-1):

$$(y_1 + y_2 + a_2) = \frac{1 - 4.77 (O_2) + 0.88 (H_2)}{1 - [(H_2) + (O_2)]} \quad (A-3)$$

where  $(H_2)$  = percent of hydrogen by volume, dry.

Since  $y_1$  is not known,  $(y_2 + a_2)$  may be calculated. Since  $a_2$  can be greater than zero only if  $(y_1 + y_2 + a_2) > 1$ , then  $a_2$  and  $y_2$  may be evaluated.

From Eq. (A-1) may also be derived the equation for  $\eta$ :

$$\eta = \frac{1 - 4.77 (O_2) - (H_2)}{1 - 4.77 (O_2) + 0.88 (H_2) + [(H_2) + (O_2) - 1] (a_2)} \quad (A-4)$$

Combustion efficiency for the test fuel only may then be defined as:

$$\epsilon = \frac{\eta (y_1 + y_2) - y_1}{y_2} \quad (A-5)$$

## GAS TEMPERATURE CALCULATION

In calculating gas temperature, dissociation was assumed to be negligible. Since dissociation is not appreciable until temperatures above 4000°R and near or above stoichiometric ratios are reached, it was neglected for the data of this report.

The final gas temperature was obtained from the following equations:

#### Enthalpy Balance

$$\begin{aligned} (m_{f_{H_2}} h_{H_2} + m_{f_{air}} h_{air} + \eta m_{f_{H_2}} Q_R)_{\text{reactants}} = \\ (m_{f_{H_2}} h_{H_2} + m_{f_{O_2}} h_{O_2} + m_{f_{N_2}} h_{N_2} + m_{f_{H_2O}} h_{H_2O})_{\text{products}} \end{aligned} \quad (A-6)$$

On the basis of one mole of  $O_2$  the mole function of the reactants and products are:

Reactants	Products
$m_{f_{H_2}} = 2(y_1 + y_2 + a_2)$	$m_{f_{H_2}} = 2(y_1 + y_2)(1 - \eta) + 2a_2$
$m_{f_{air}} = 4.77$	$m_{f_{O_2}} = 1 - (y_1 + y_2)\eta$
	$m_{f_{N_2}} = 3.77$
	$m_{f_{H_2O}} = 2\eta(y_1 + y_2)$

Enthalpy equations for the products in the form  $h = a + bT_t + cT_t^2$  were developed for  $H_2$ ,  $O_2$ ,  $N_2$ , and  $H_2O$  from 1200 to 4000°R using enthalpy data from Ref. 13:

$$h_{H_2} = -3184 + 6.2596 T_t + 0.2683 \times 10^{-3} T_t^2 \text{ Btu/lb mole } (\pm 10)^* \quad (A-7)$$

$$h_{O_2} = -2818 + 6.1636 T_t + 0.4786 \times 10^{-3} T_t^2 \text{ Btu/lb mole } (\pm 300) \quad (A-8)$$

$$h_{N_2} = -3941 + 6.9532 T_t + 0.2411 \times 10^{-3} T_t^2 \text{ Btu/lb mole } (\pm 40) \quad (A-9)$$

$$h_{H_2O} = -4277 + 7.441 T_t + 0.682 \times 10^{-3} T_t^2 \text{ Btu/lb mole } (\pm 60) \quad (A-10)$$

In these equations,  $h = 0$  at 524°R.

Similar equations for the reactants were developed:

$$h_{H_2} = -3686 + 6.984 T_{t_{H_2}} (\pm 10)^* \quad T_t = 600 - 1000^\circ R \quad (A-11)$$

$$h_{air} = -4348 + 7.617 T_{t_{air}} (\pm 20) \quad T_t = 1300 - 1600^\circ R \quad (A-12)$$

where  $h = 0$  at 524°R and  $Q_R = 104100$  Btu/lb mole at 524°R. (Ref. 14)

---

\*The equation fits the tables (Ref. 13) to this tolerance expressed as Btu/lb mole.



These equations may be combined to form the quadratic equation:

$$\begin{aligned}
 & [ 1.3876 + 0.5366 (y_1 + y_2 + a_2) + 0.3488 \eta (y_1 + y_2) ] 10^{-3} T_t^2 \\
 & + [ 32.3772 + 12.5192 (y_1 + y_2 + a_2) - 3.8008 \eta (y_1 + y_2) ] T_t \quad (A-13) \\
 & - [ -3063 - 998 (y_1 + y_2 + a_2) + 207600 \eta (y_1 + y_2) \\
 & + 36.333 T_{t_{air}} + 13.968 T_{t_{H_2}} (y_1 + y_2 + a_2) ] = 0
 \end{aligned}$$

These equations for a  $H_2$  - air reaction mixture are accurate to  $\pm 5^\circ R$ .

Three gas temperatures may be calculated:

1. Preheater only ( $T_{t_0}$ ) where  $y_2$  and  $a_2$  are 0 and  $\eta = 1.0$ .
2. Preheater plus test fuel without test fuel combustion ( $T_{t_0}$ ) where  $\eta (y_1 + y_2) = y_1$ .
3. Preheater plus test fuel with test fuel combustion ( $T_t$ ) as written in Eq. (A-13).

Thus, the properties of the reacting gas that can be determined from a  $H_2$  -  $O_2$  analysis on a dry basis, assuming a quenched reaction, are as follows:

1. Fuel-air ratio (partially burned or unburned).
2. Combustion efficiency.
3. Gas temperature from fuel-air ratio and combustion efficiency.

## ERROR ANALYSIS

Error analysis was based on an estimated 95-percent probability that the measurements lay inside a certain interval. For measured data, the interval was taken as that within which repeatable observations could be made. For calculations the plus or minus increment ( $\Delta$ ) was calculated from the data  $\Delta$ 's. A comparison of Table A-1 with Figs. 16, 19, 20, and 21 will verify the validity of the estimated 95-percent probability.

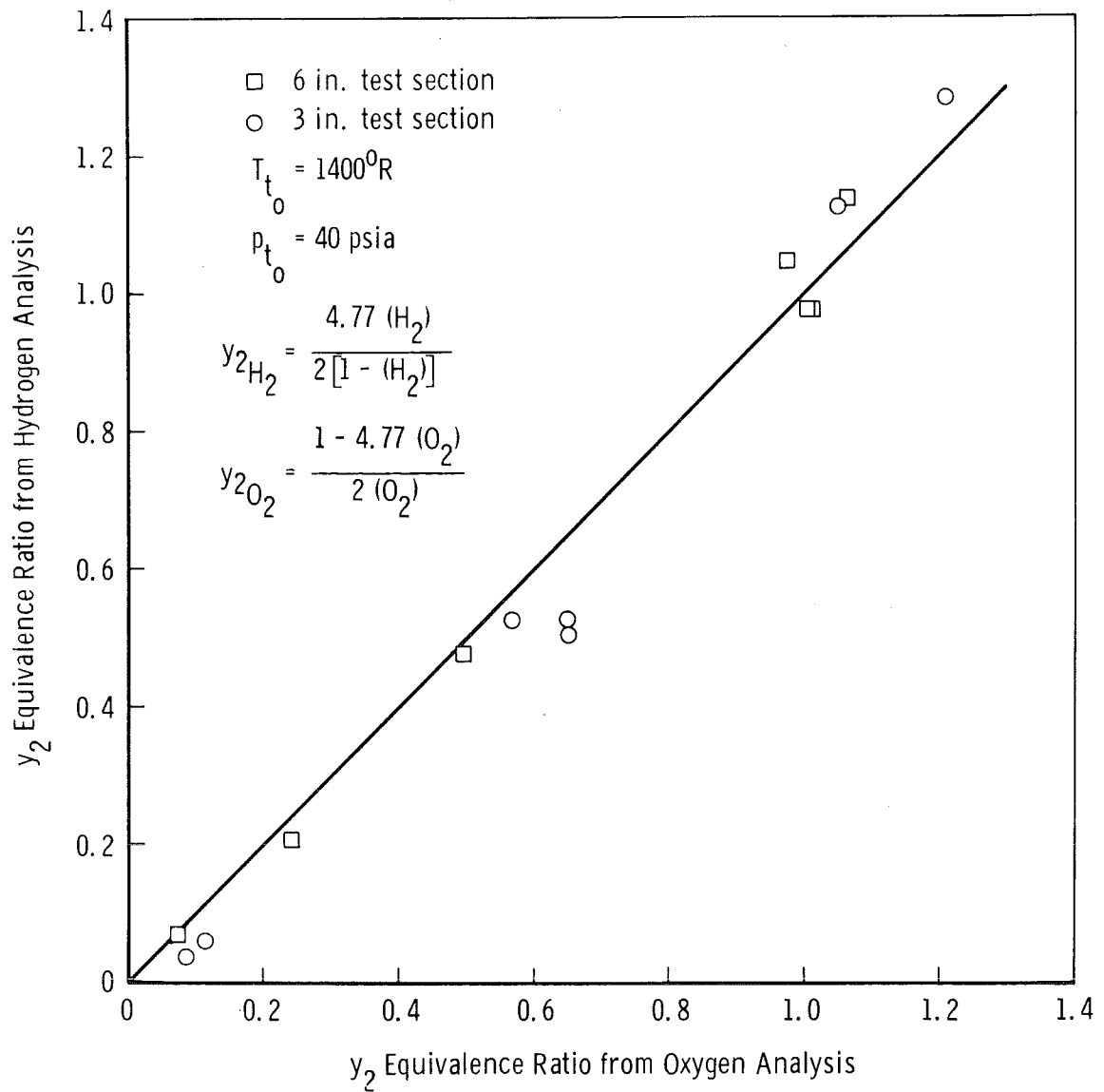
Table A-1 was based on  $\epsilon$  values near 30 percent, about mid range.

TABLE A-1

PARAMETER	REFERRED SOURCE	95. PERCENT CONFIDENCE LIMIT
$p_t'$ (P.H. & Fuel)	Data	$\pm 0.6$ %
$p_t'$ (P.H. Only)	Data	$\pm 0.6$
$(p_t' \text{ P.H. \& Fuel}) / (p_t' \text{ P.H. Only})$	$p_t'$ data	$\pm 1.2$
$H_2$	Data	$\pm 1.6$
$O_2$	Data	$\pm 0.8$
$y_1$	$H_2, O_2$	$\mp 0.7$
$y_1 + y_2$	$H_2, O_2, y_1$	$\mp 7$
$\eta$	$H_2, O_2$	$\mp 6$
$\epsilon$	$\eta, y_1, y_2$	$\mp 9$
$T_{t_0}$	$y_1$	$\mp 2$
$T_t$	$y_1 (y_1 + y_2) \eta$	$\mp 5$
$T_t/T_{t_0}$	$T_{t_0}, T_t$	$\mp 7.5$

Reliability of the  $H_2$  and  $O_2$  analysis may be gaged by plotting fuel-air equivalence ratio for unburned fuel as calculated by Eqs. (A-3) and (A-4). A plot of this nature is shown in Fig. A-1. An error or deviation of both measurements can cancel out or cause dispersion of data from the "perfect agreement" line.





**Fig. A-1 Correlation of Fuel Concentration from Hydrogen and Oxygen Analysis**



## APPENDIX B

ANALYSIS OF CHEMICAL REACTION QUENCH RATES  
IN THE GAS SAMPLING PROBE

Since much of the data and conclusions in this report are based on sampling of the gas in a burning stream, the question arises as to just how rapidly quenching of the chemical reaction occurs. That quenching occurs is well established by the fact that combustion efficiencies, calculated based on the gas analysis, ranged from zero percent to approximately 90 percent. The reaction is started if any combustion can be detected. The calculated combustion efficiency indicates that the gas entered the probe (Fig. B-1) at some state of reaction completion, and was quenched inside the probe between the inlet orifice and a point downstream, based on the following analysis:

- a. When the probe was positioned in the supersonic flow ahead of the normal shock or just aft of the normal shock where no emission was observed, the calculated combustion efficiency was zero. This was found to be true even though the calculated combustion efficiency one inch downstream was as high as 60 to 70 percent. This observation indicates that quenching occurred faster than the reaction could achieve a measurable start, or less than 3 microseconds (Fig. 1b).
- b. When a straight tube probe inlet was used instead of the choked orifice of Fig. B-1, no quench occurred at all, and the reaction proceeded to completion inside the probe.
- c. Analysis of the probe interior flow after the gas had entered indicates that the flow is choked and expands supersonically. The two possible cases are:
  1. Separated flow (as shown in Fig. B-1) where the gas expands to about  $M = 1.7$  or higher and dissipates into the surrounding cooler gas. (Expansion and quenching occurs in less than 1 microsecond. The flow is about 85 percent diffused into the surrounding cool gases in 3 microseconds.)
  2. Fully developed expansion, which is possible with the 6 to 7:1 pressure ratio available. (In this case, the flow expands to Mach 3.5, and the reaction is quenched in less than 1 microsecond. This flow shocks down in about 5 diameters (Ref. 15). The changes in static temperature when passing the quenched gas through the shocks are not

clear. Here again, if re-ignition did occur, it is expected that its presence would become known in the gas analysis.)

The conclusion reached from this analysis is that quenching of the reaction must occur within a period of 2 to 3 microseconds.

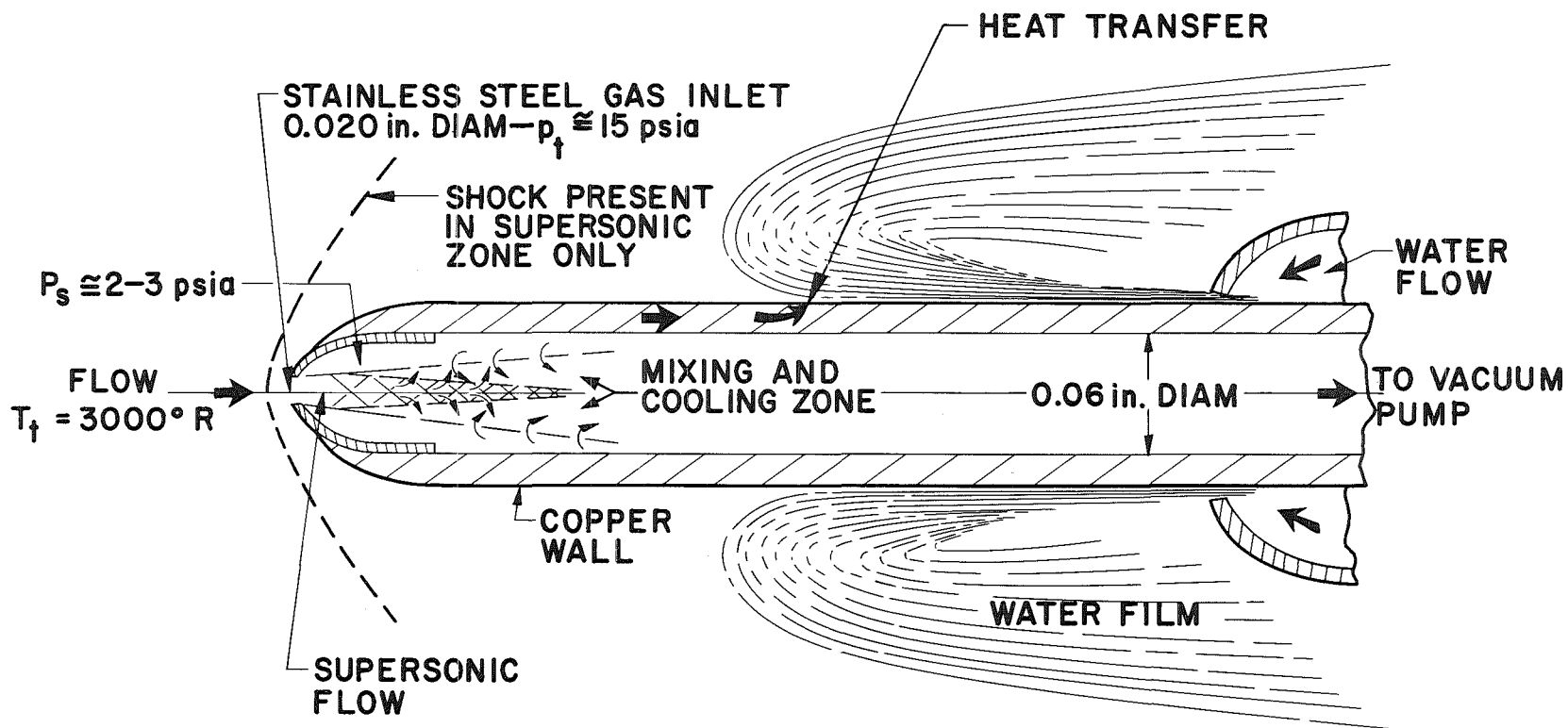


Fig. B-1 Schematic of Gas Sampling Probe Quench Analysis





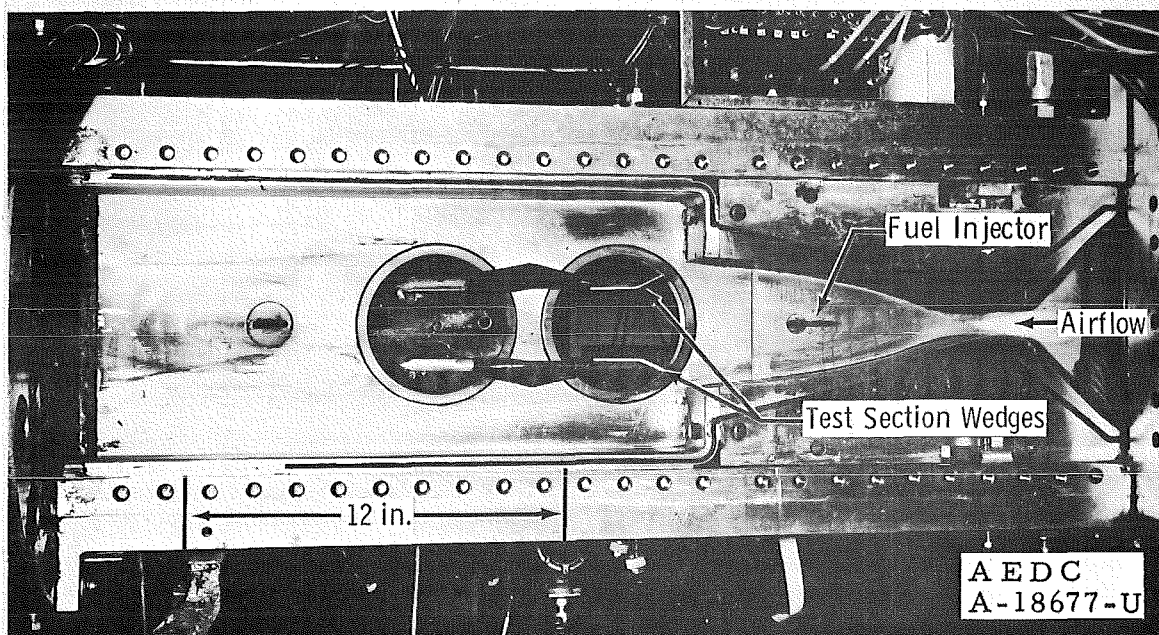
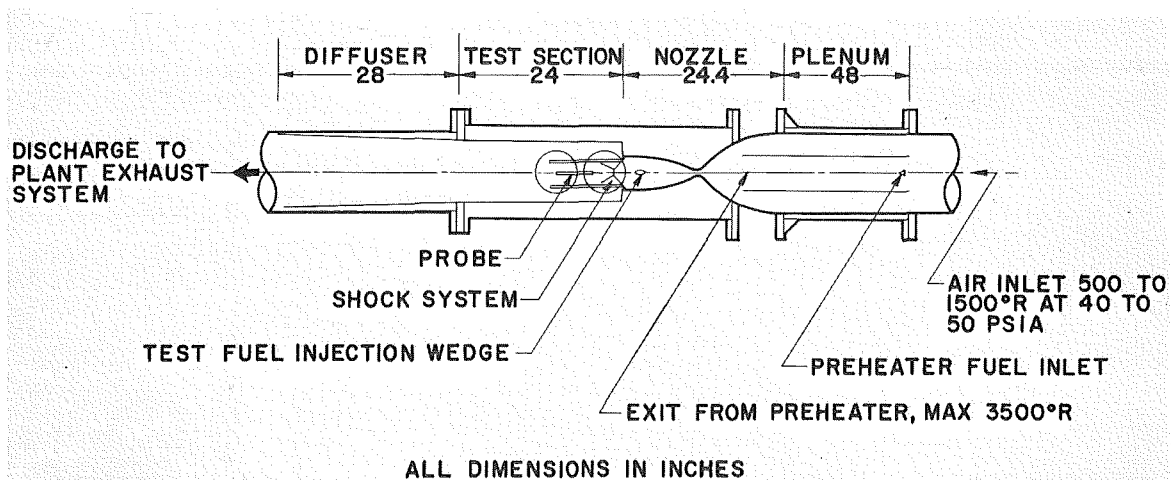


Fig. 1 Supersonic Combustion Tunnel with Normal Shock Configuration

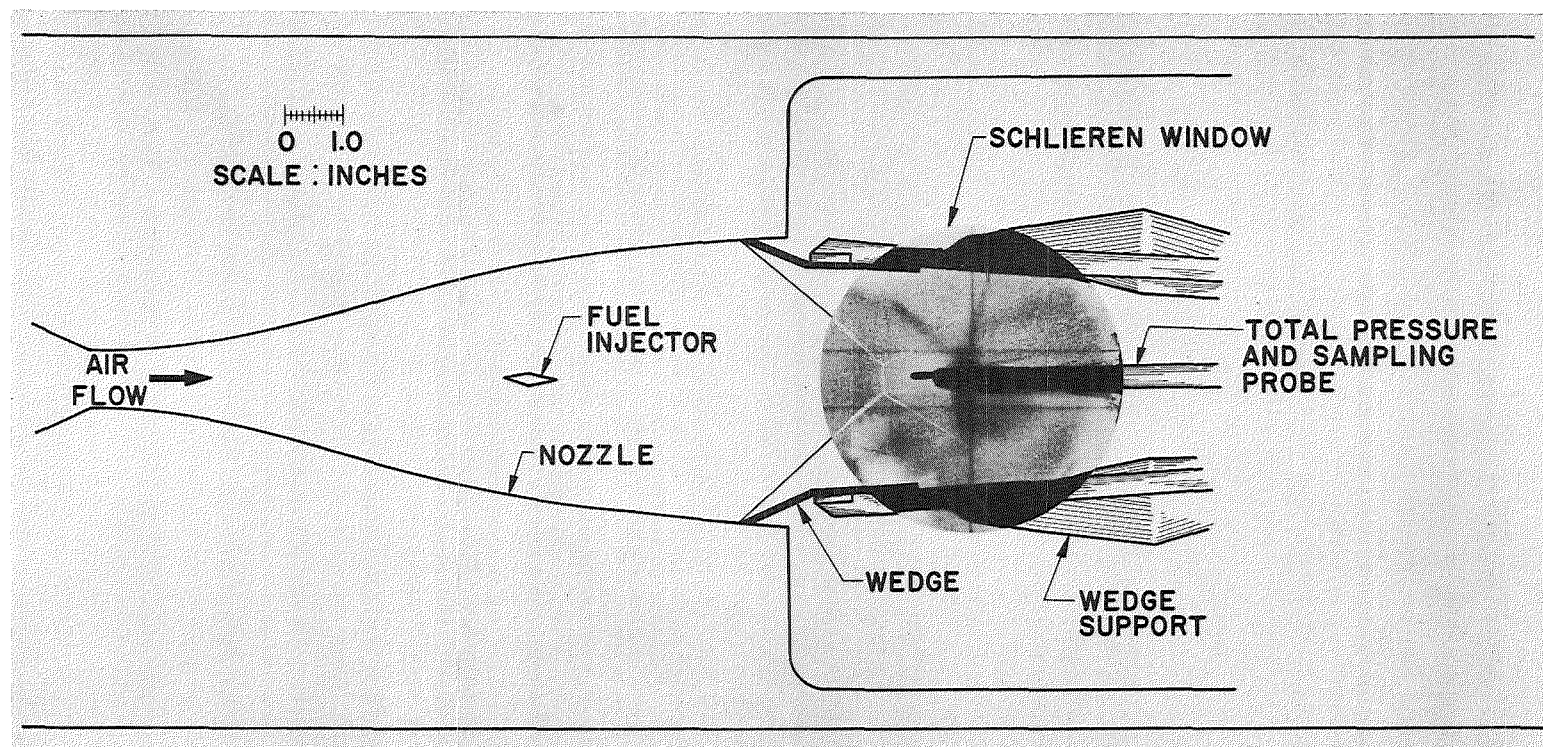


Fig. 2 Schematic of Nozzle and Test Section Showing Normal Shock Configuration with Schlieren Photo of Shock System

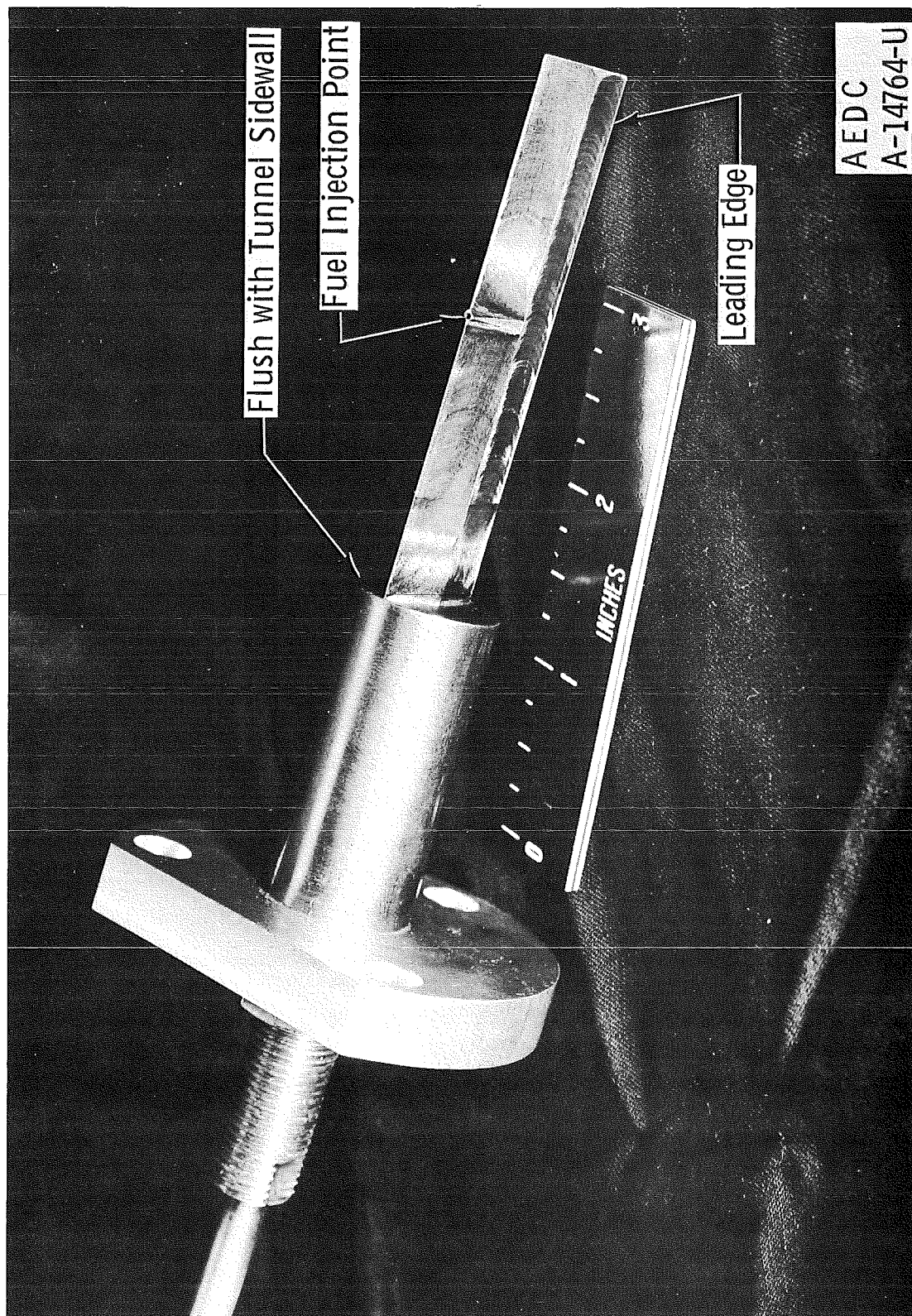


Fig. 3 Fuel Injection Wedge



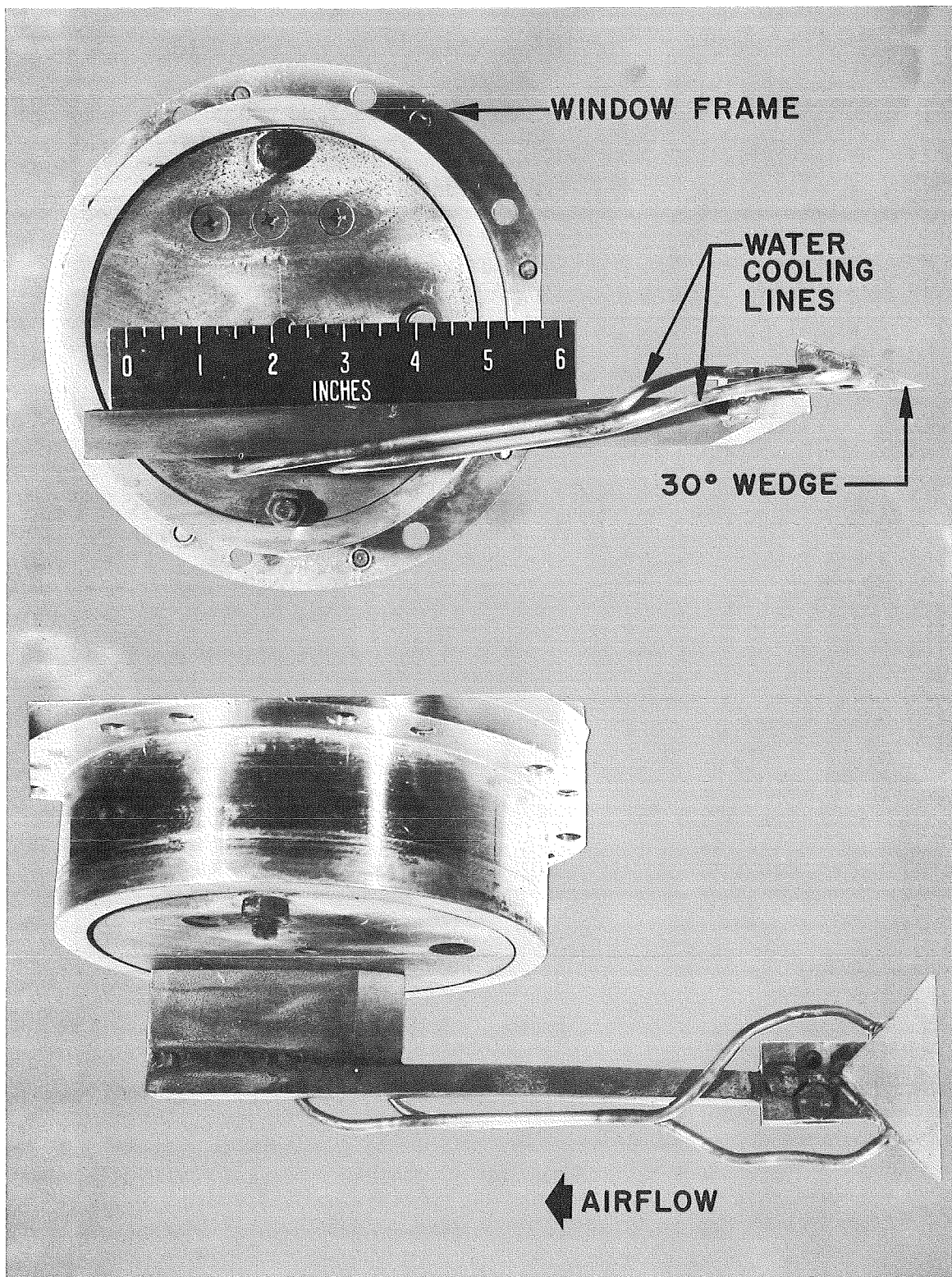


Fig. 4 Single Wedge Used to Produce Oblique Shock Waves

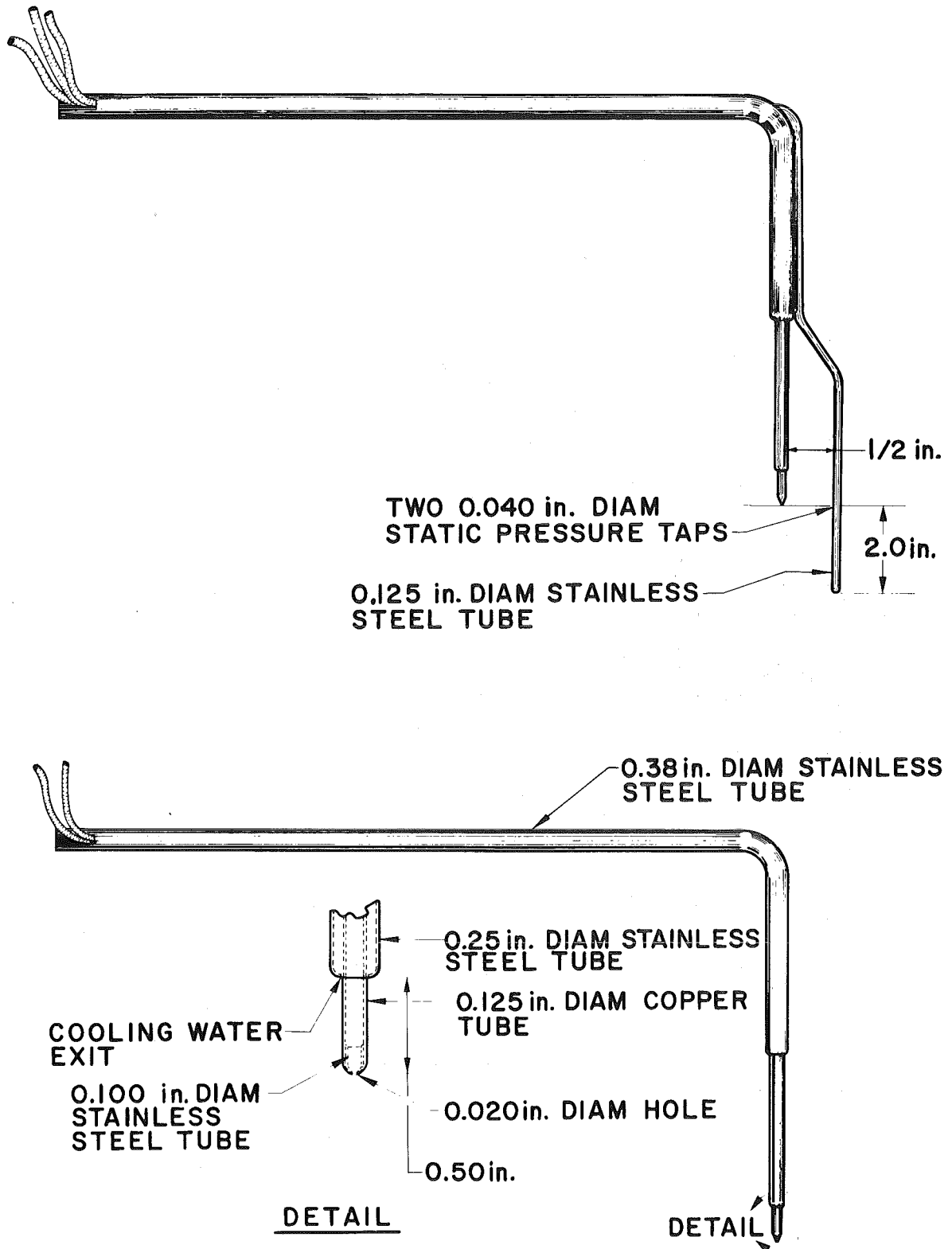


Fig. 5 Pressure and Sampling Probe

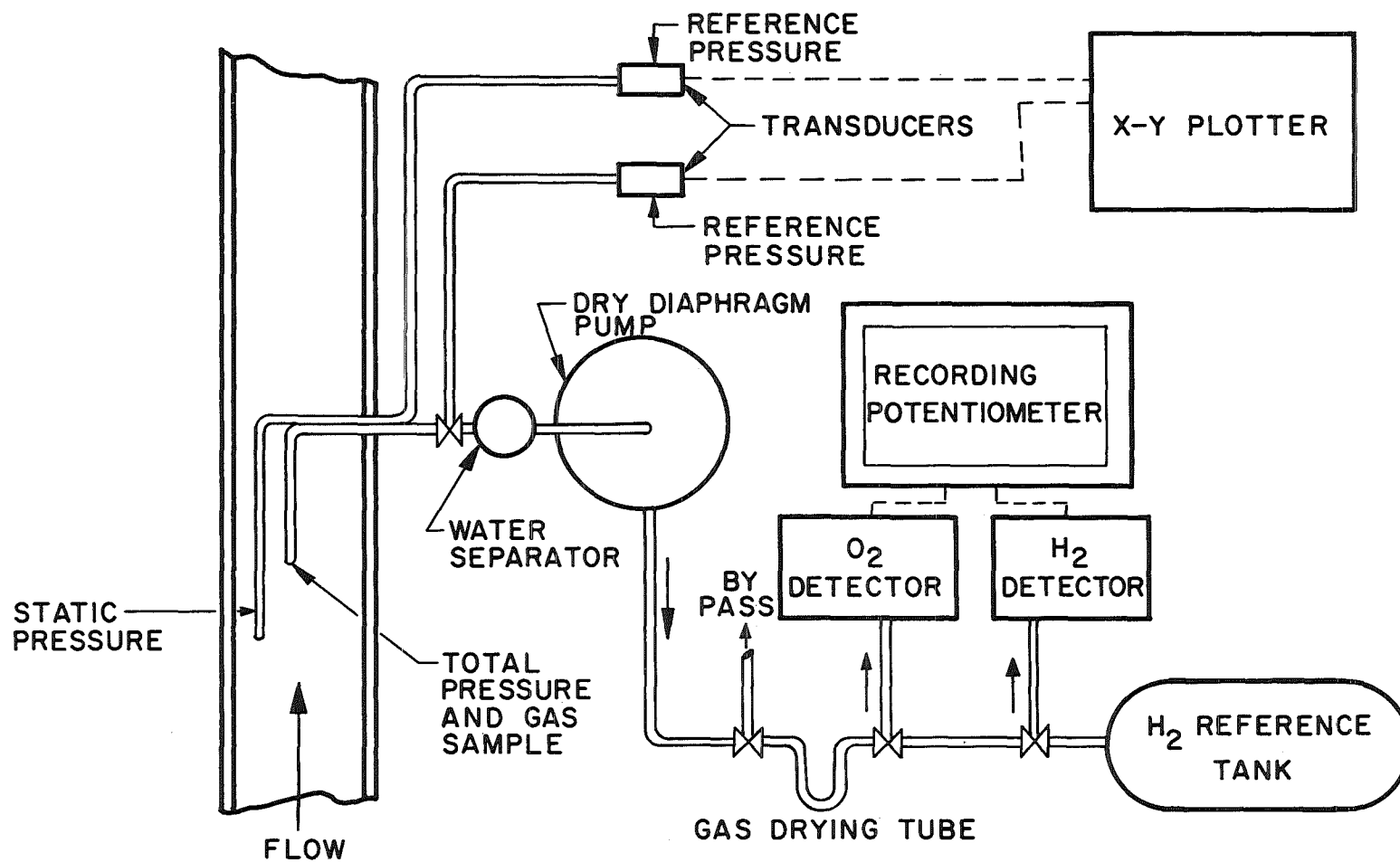


Fig. 6 Schematic of Pressure and Gas Sampling Equipment

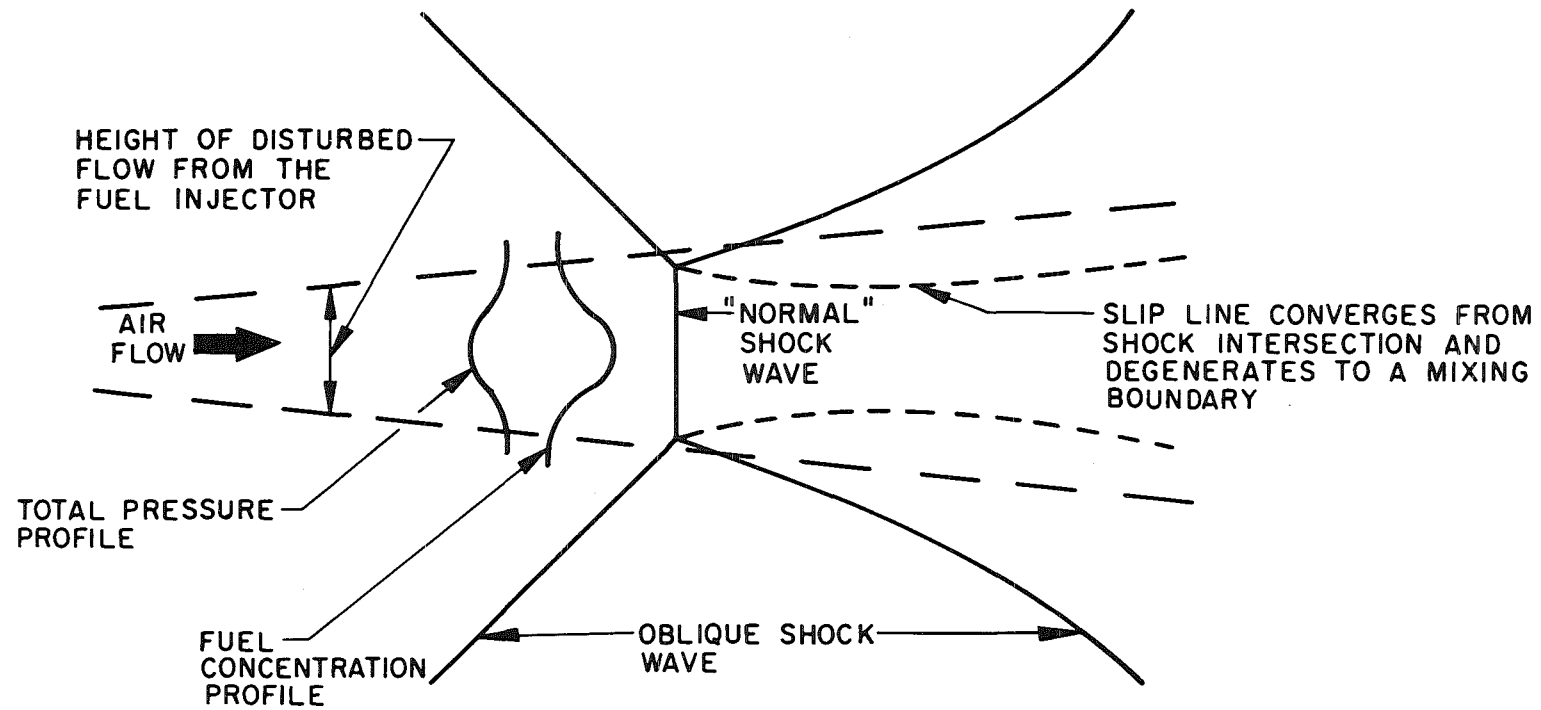


Fig. 7 Mach Reflected Normal Shock Wave



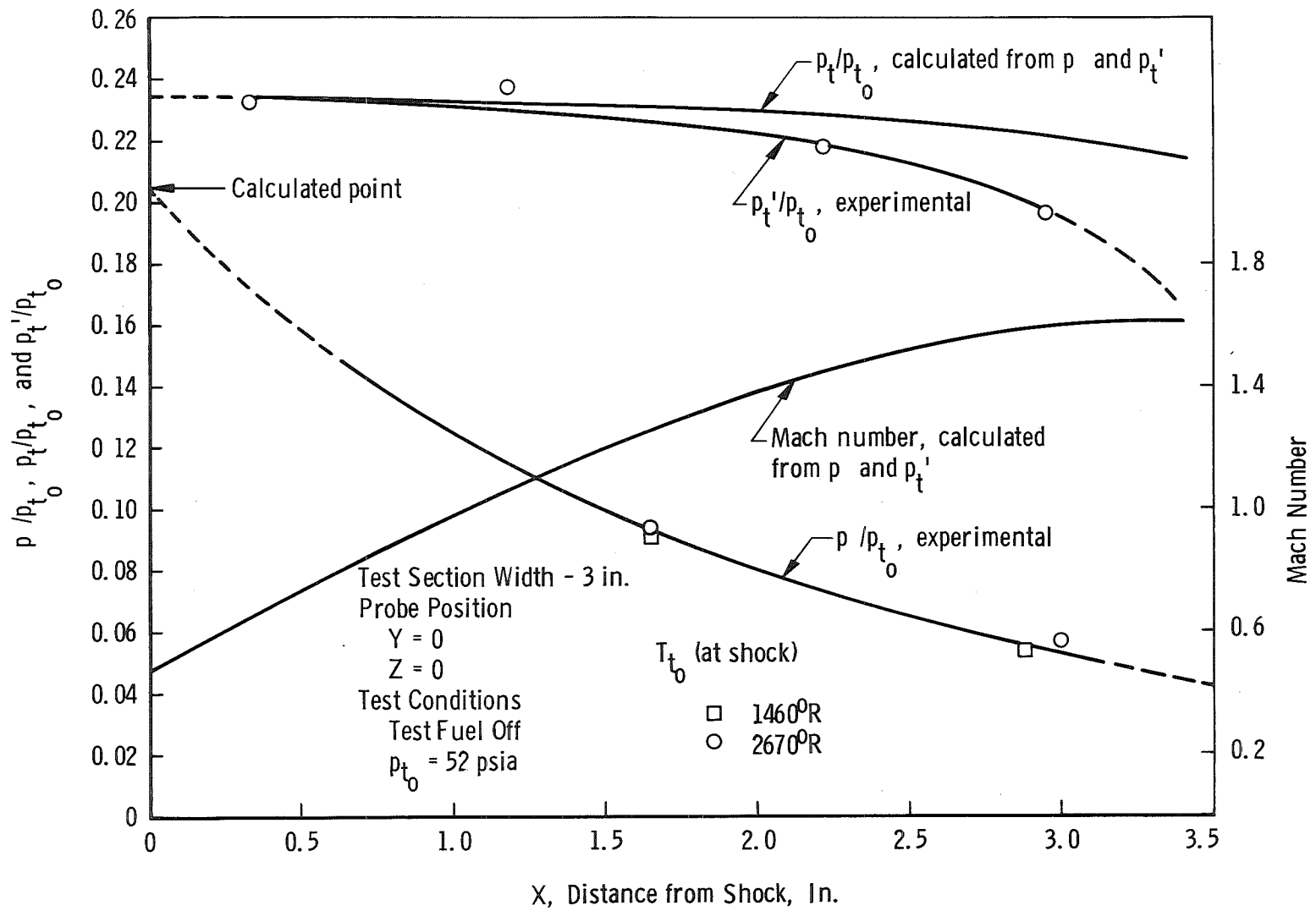


Fig. 8 Variation of Flow Parameters on Tunnel Centerline

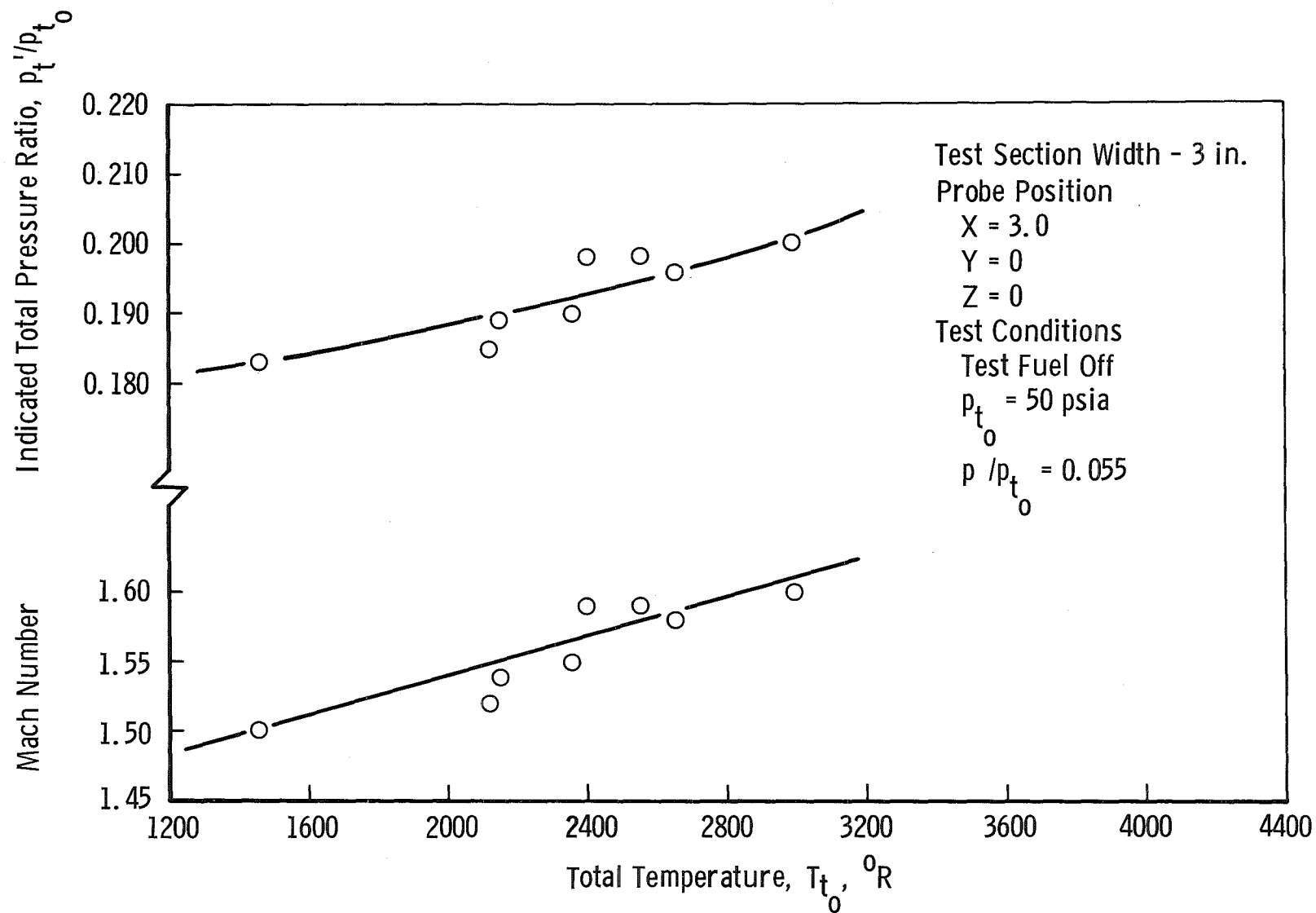


Fig. 9 Effect of Preheater Temperature on Flow Parameters on Tunnel Centerline

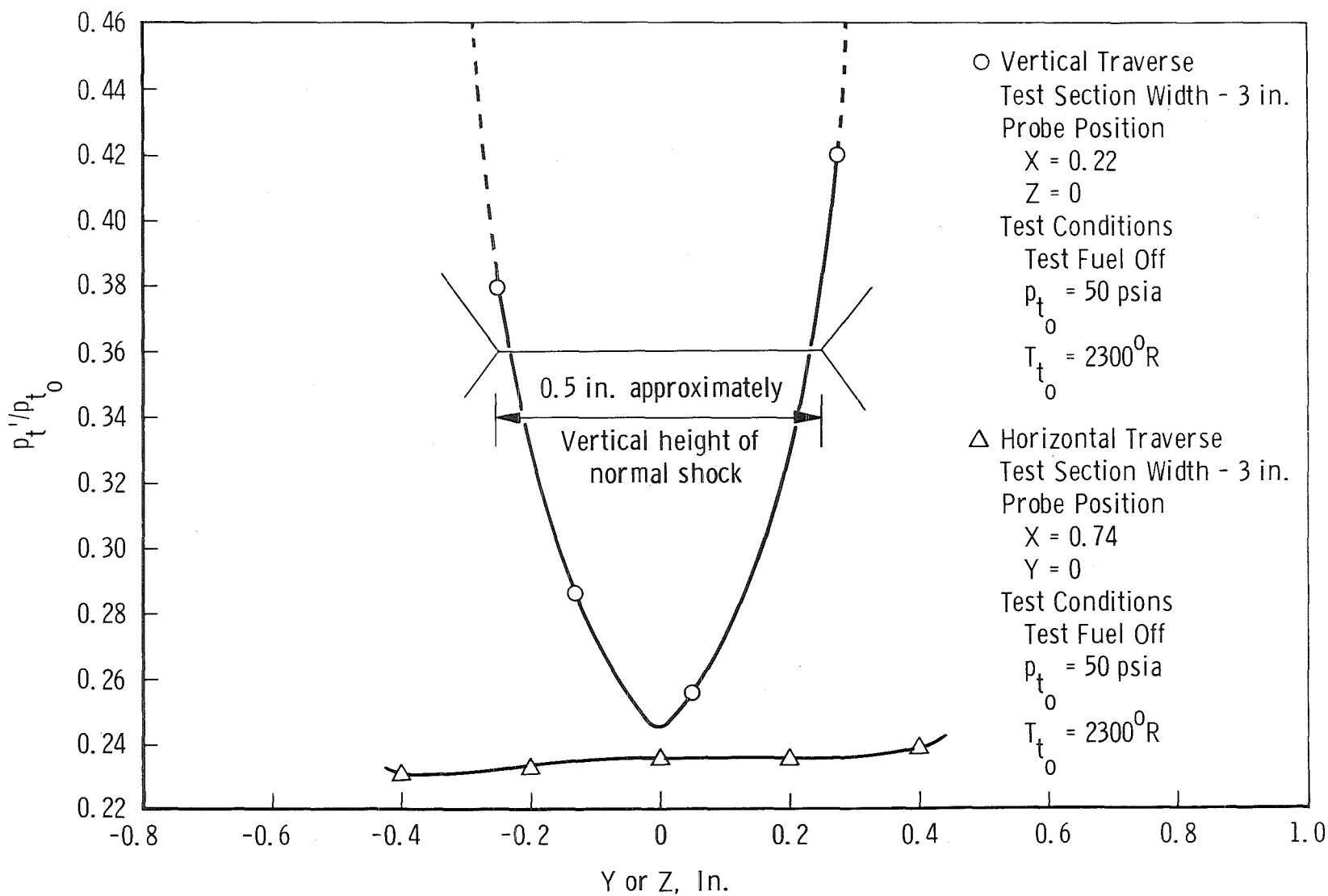
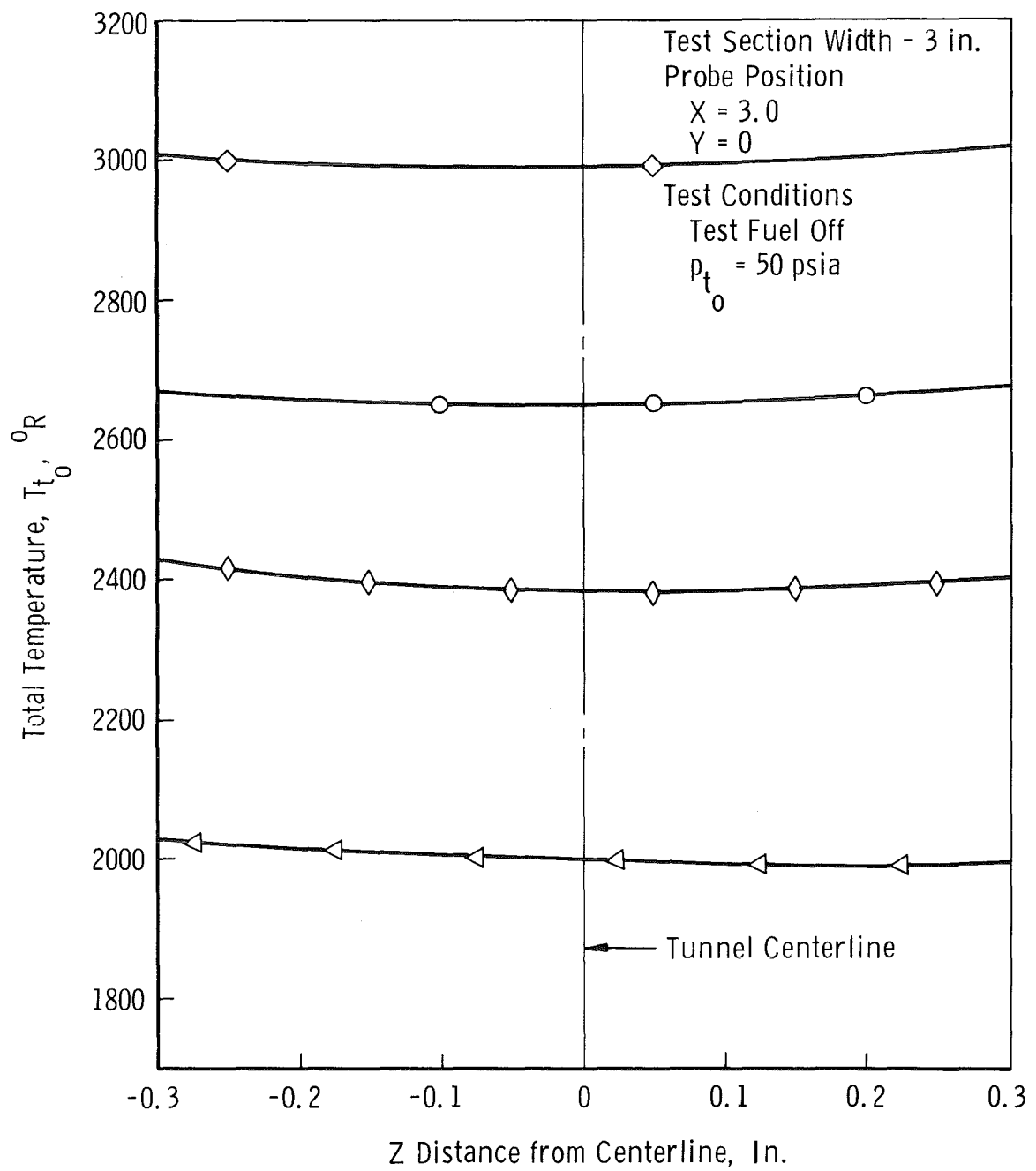
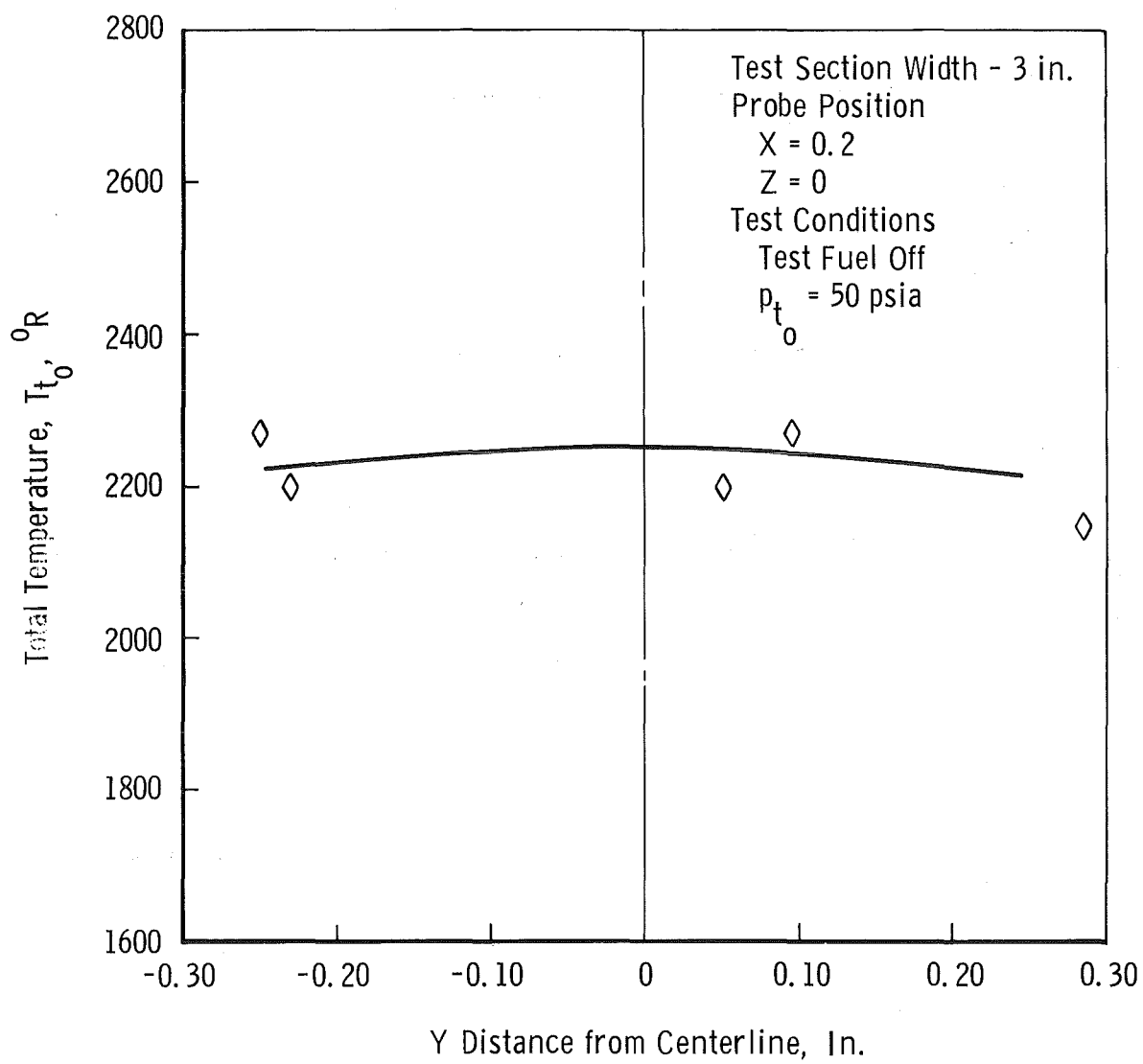


Fig. 10 Total Pressure Profile Aft of Normal Shock Wave



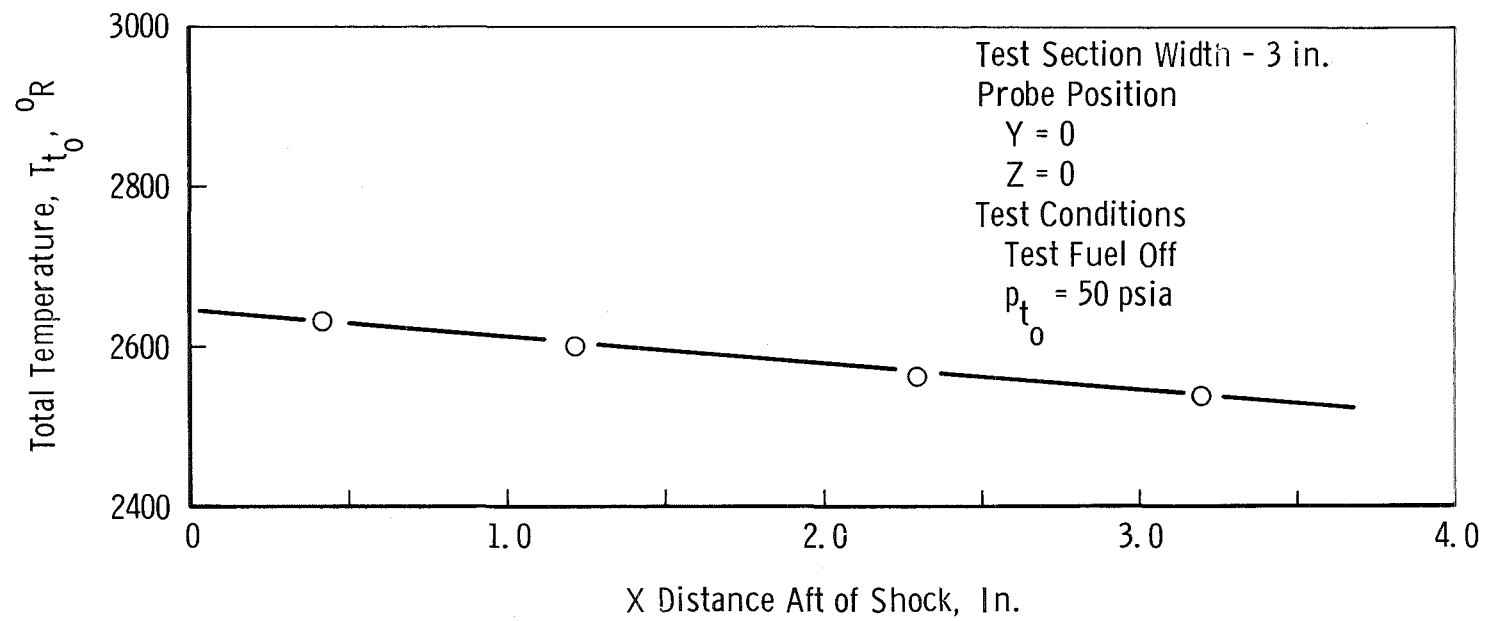
a. Horizontal

Fig. 11 Total Temperature Traverse - No Test Fuel



b. Vertical

Fig. 11 Continued



c. Axial

Fig. 11 Concluded

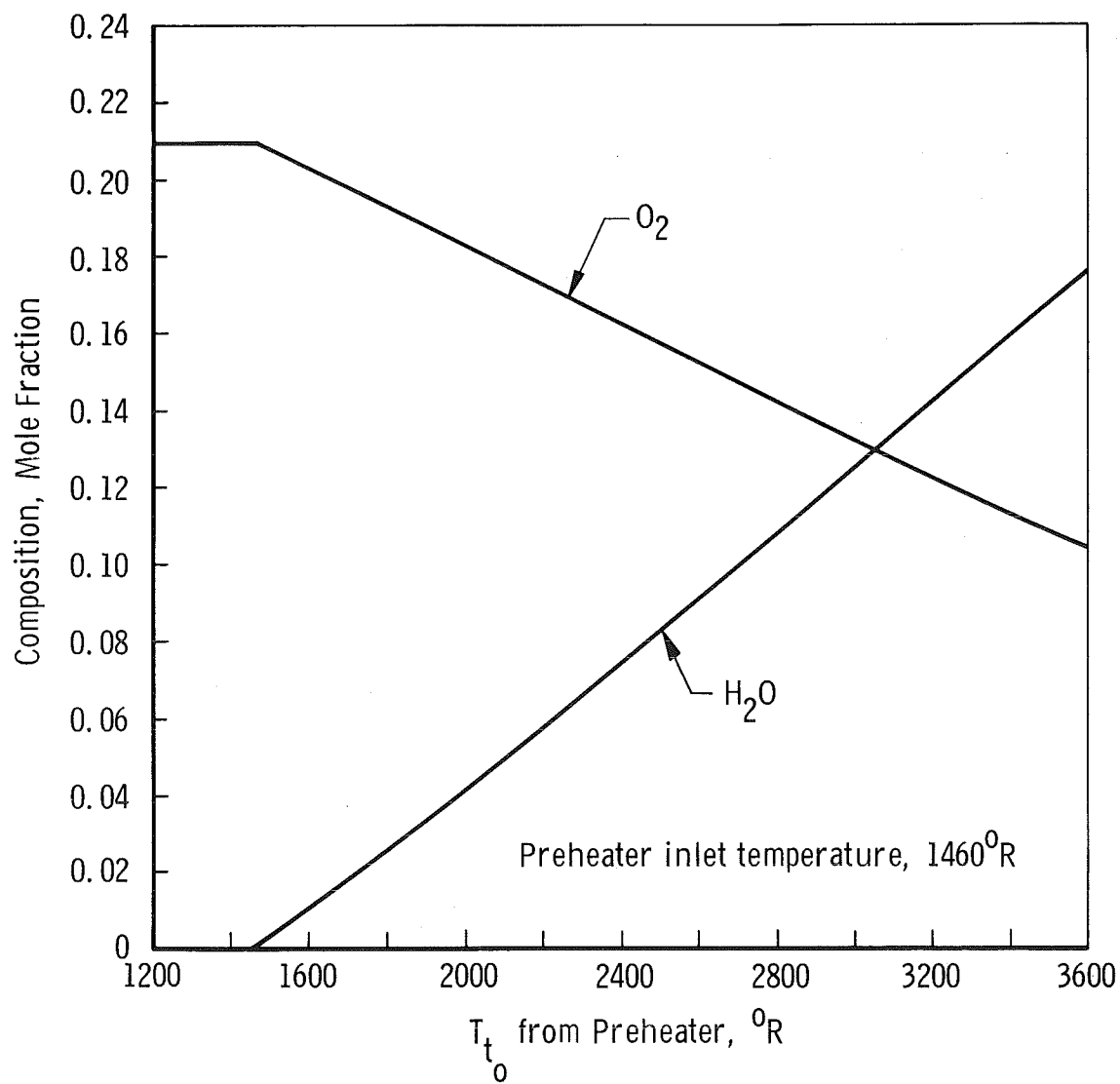


Fig. 12 Preheater Gas Composition vs Total Temperature

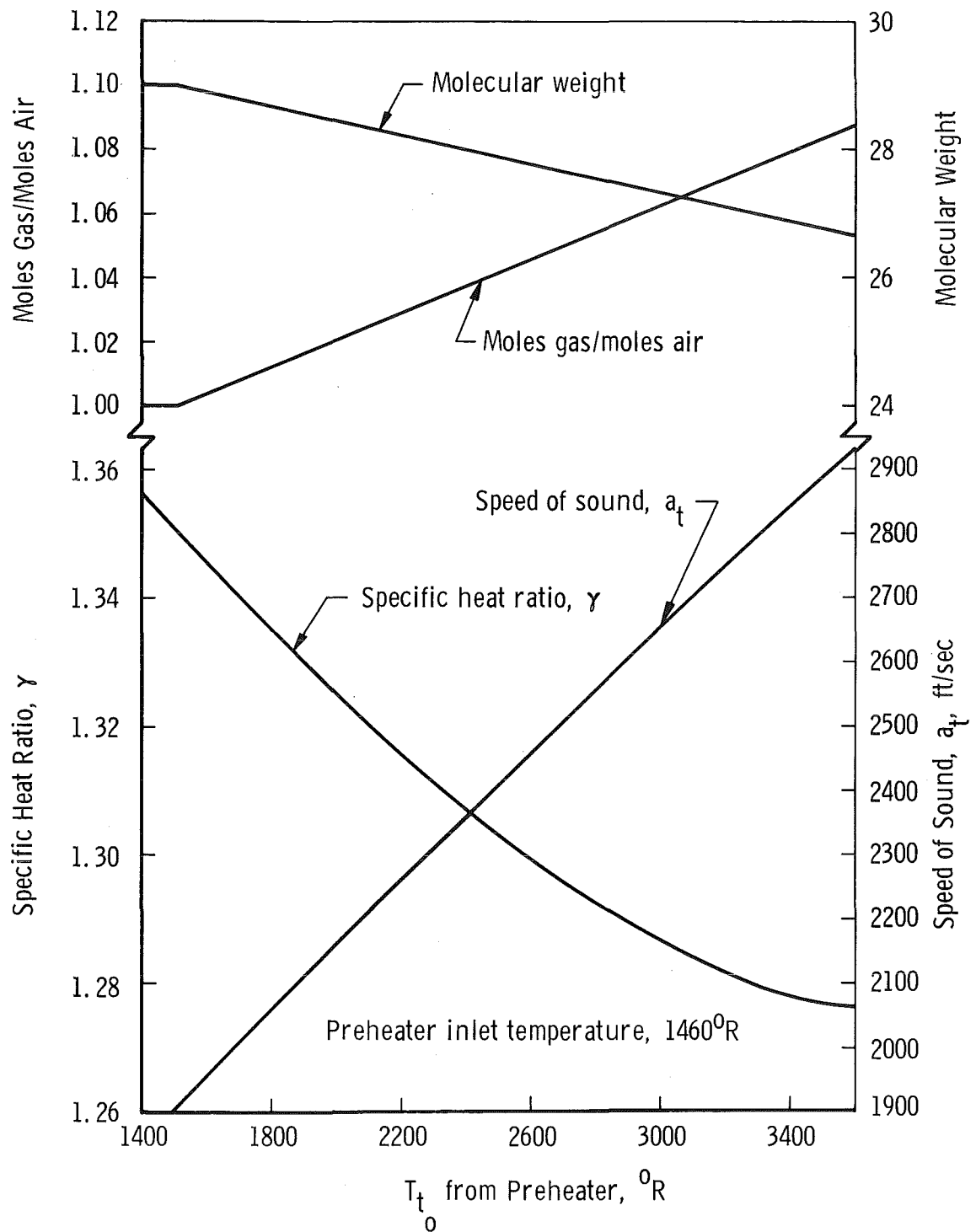
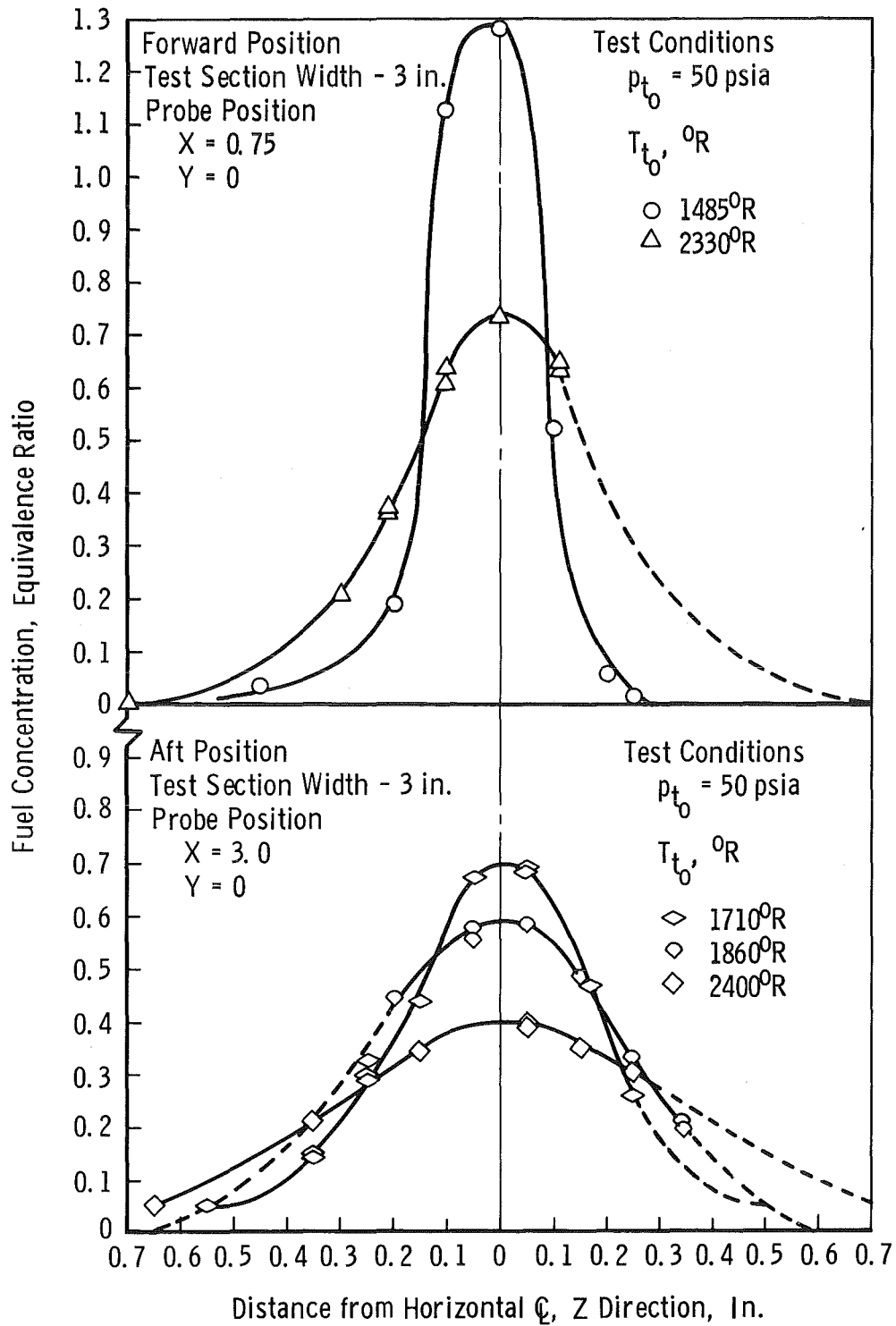


Fig. 13 Preheater Gas Properties vs Total Temperature



Fig. 14 Fuel Distribution as a Function of  $T_{t0}$

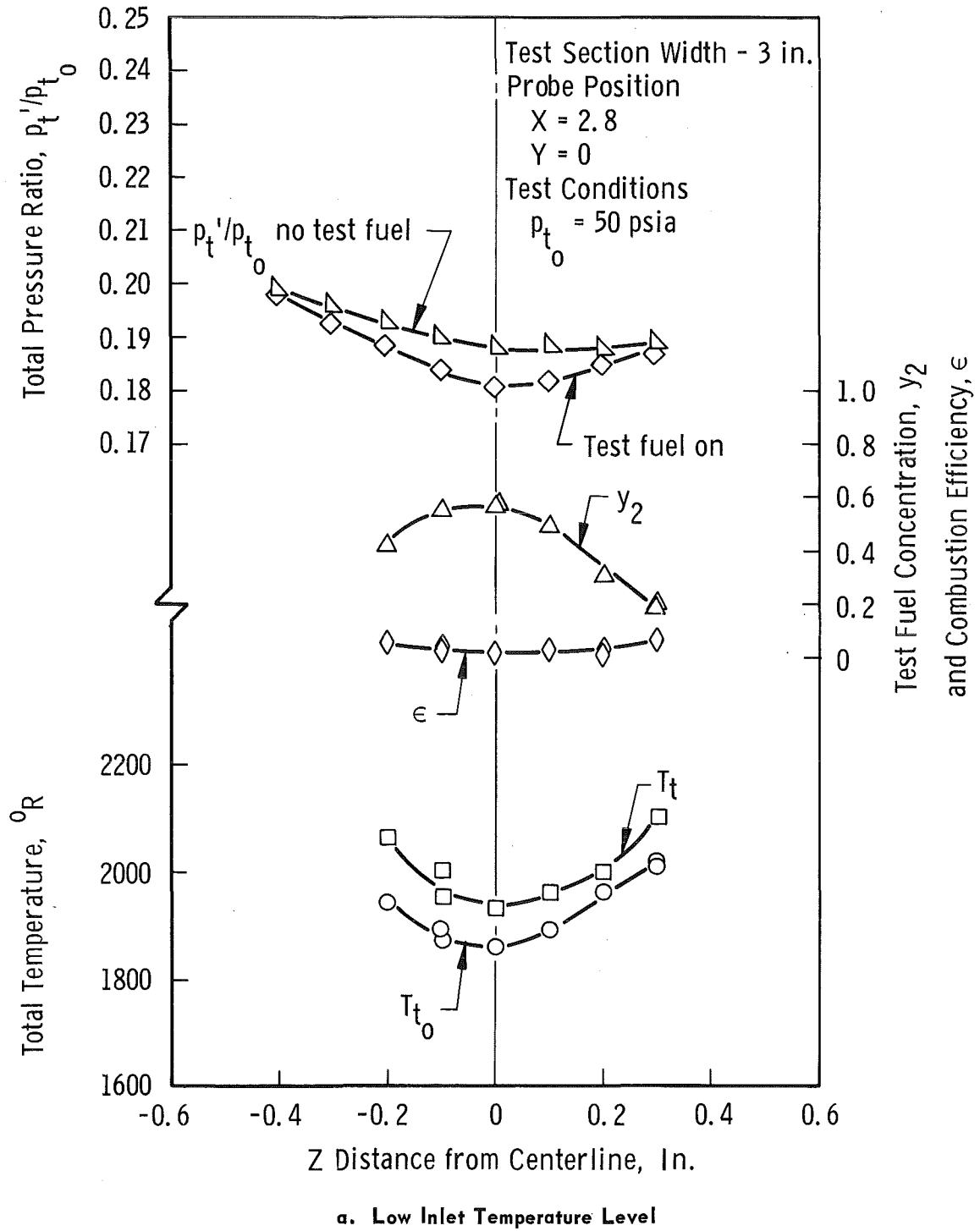
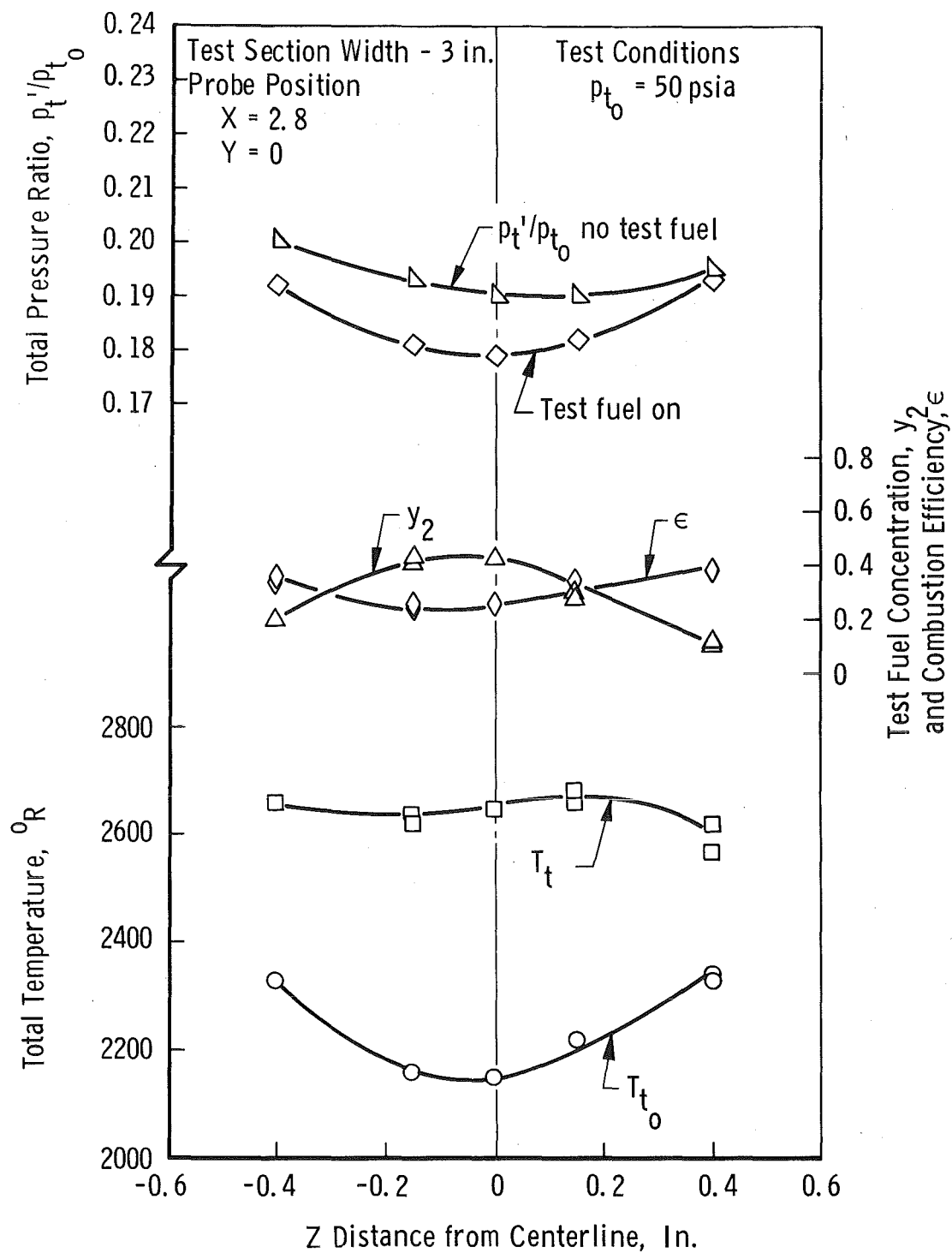
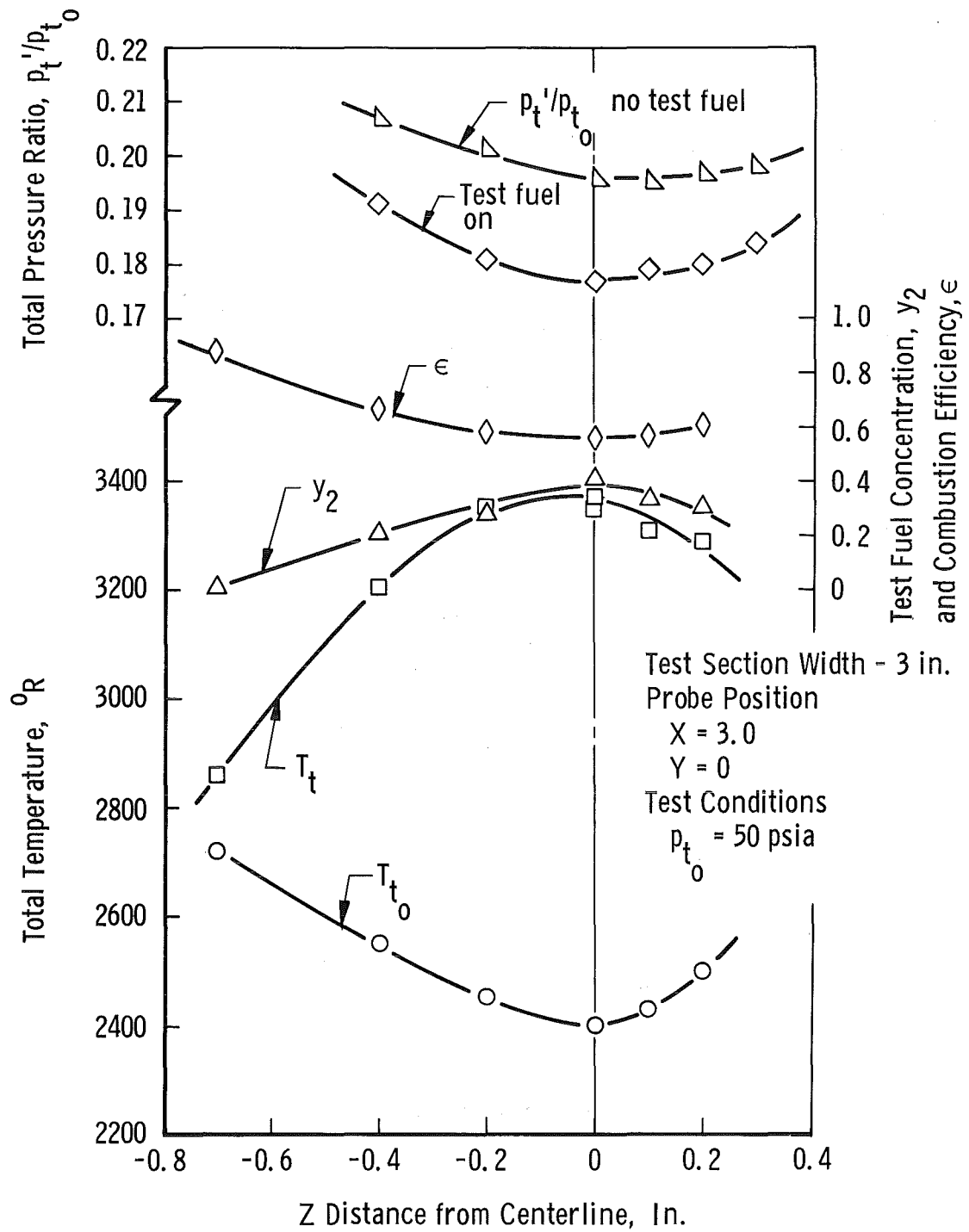


Fig. 15 Variation of Combustion Parameters across the Tunnel Width



b. Medium Inlet Temperature Level

Fig. 15 Continued



c. High Inlet Temperature

Fig. 15 Concluded

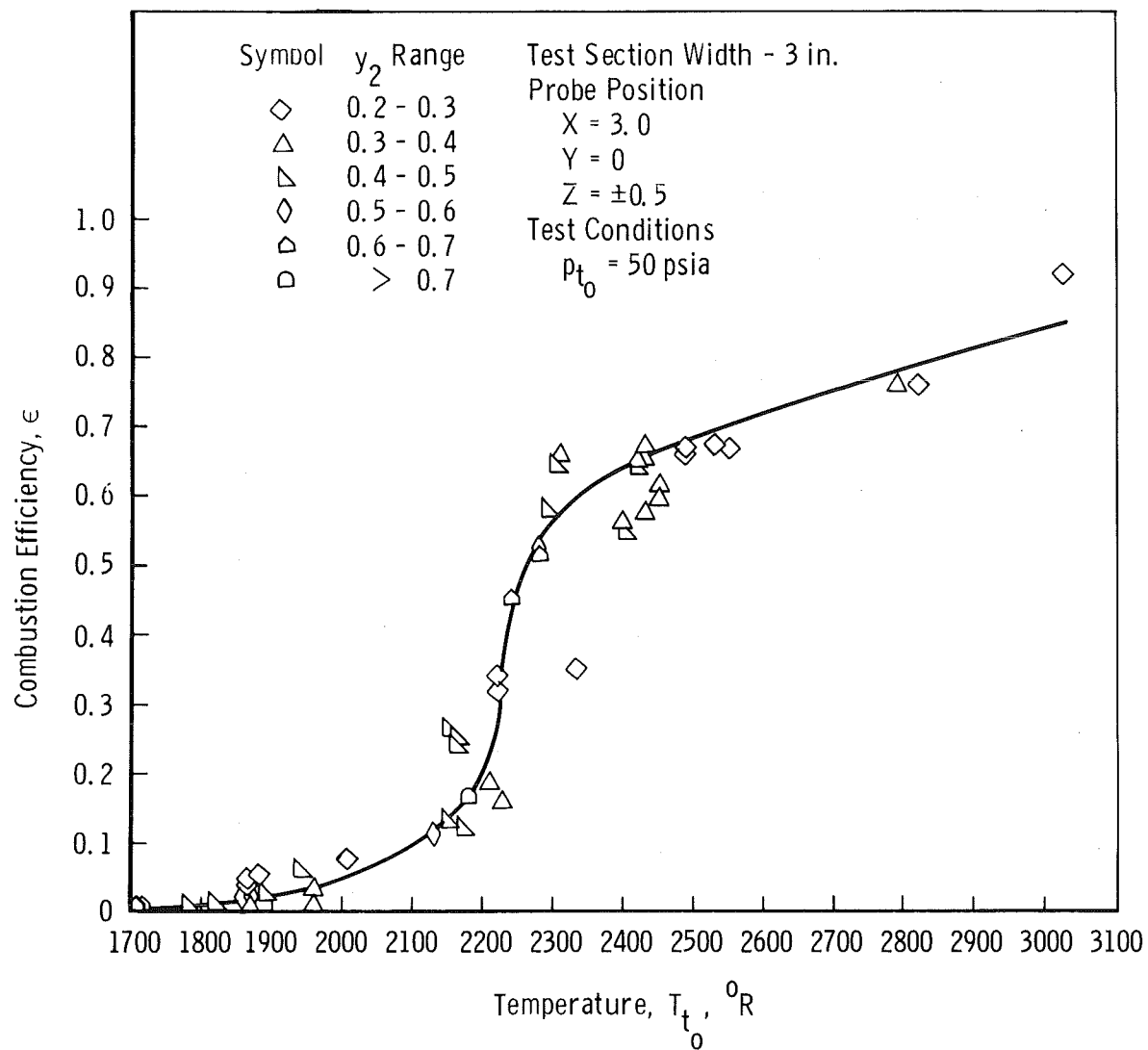


Fig. 16 Combustion Efficiency as a Function of Inlet Temperature

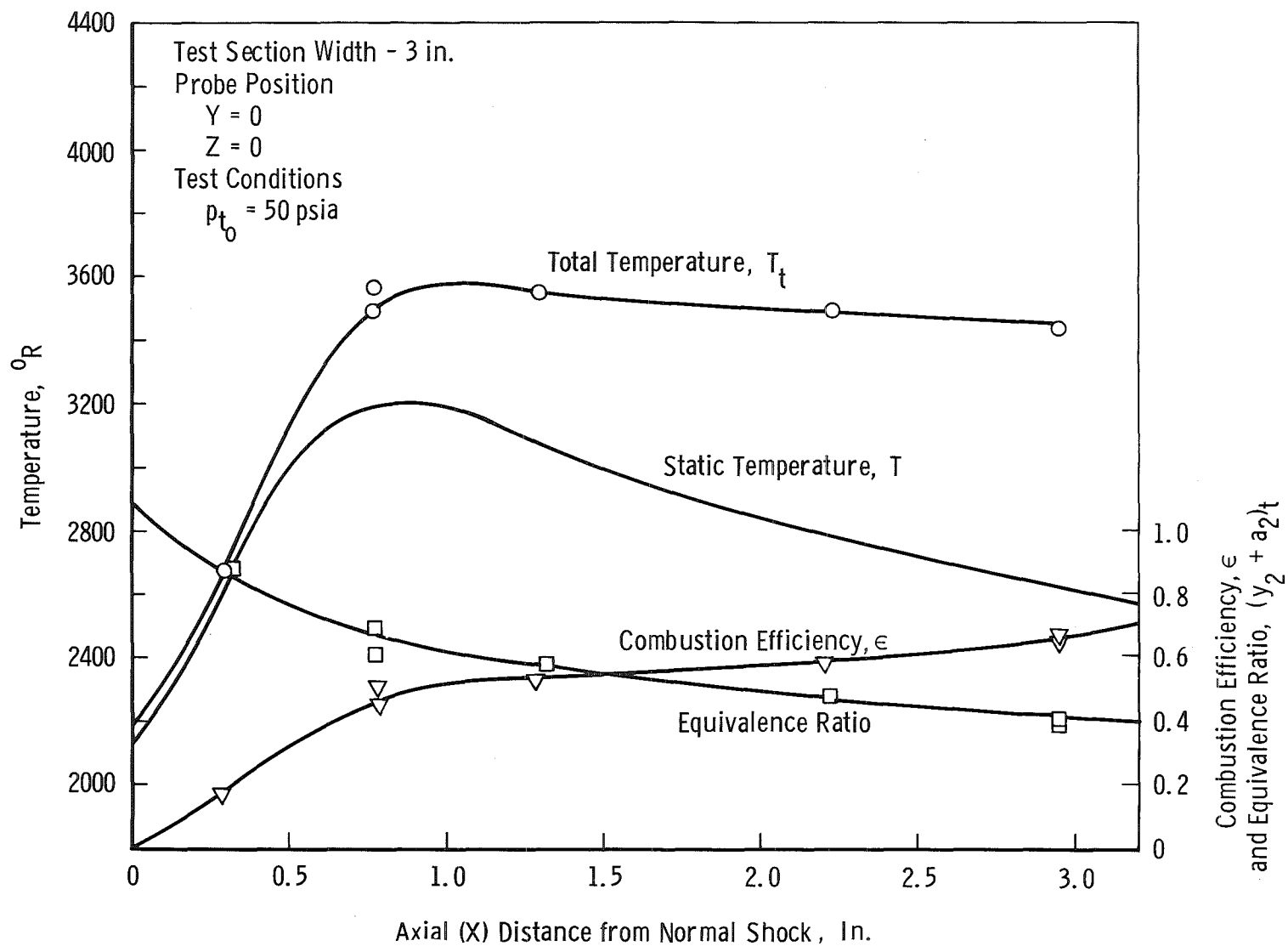


Fig. 17 Variation of Flow Parameters on Centerline with Test Fuel Combustion

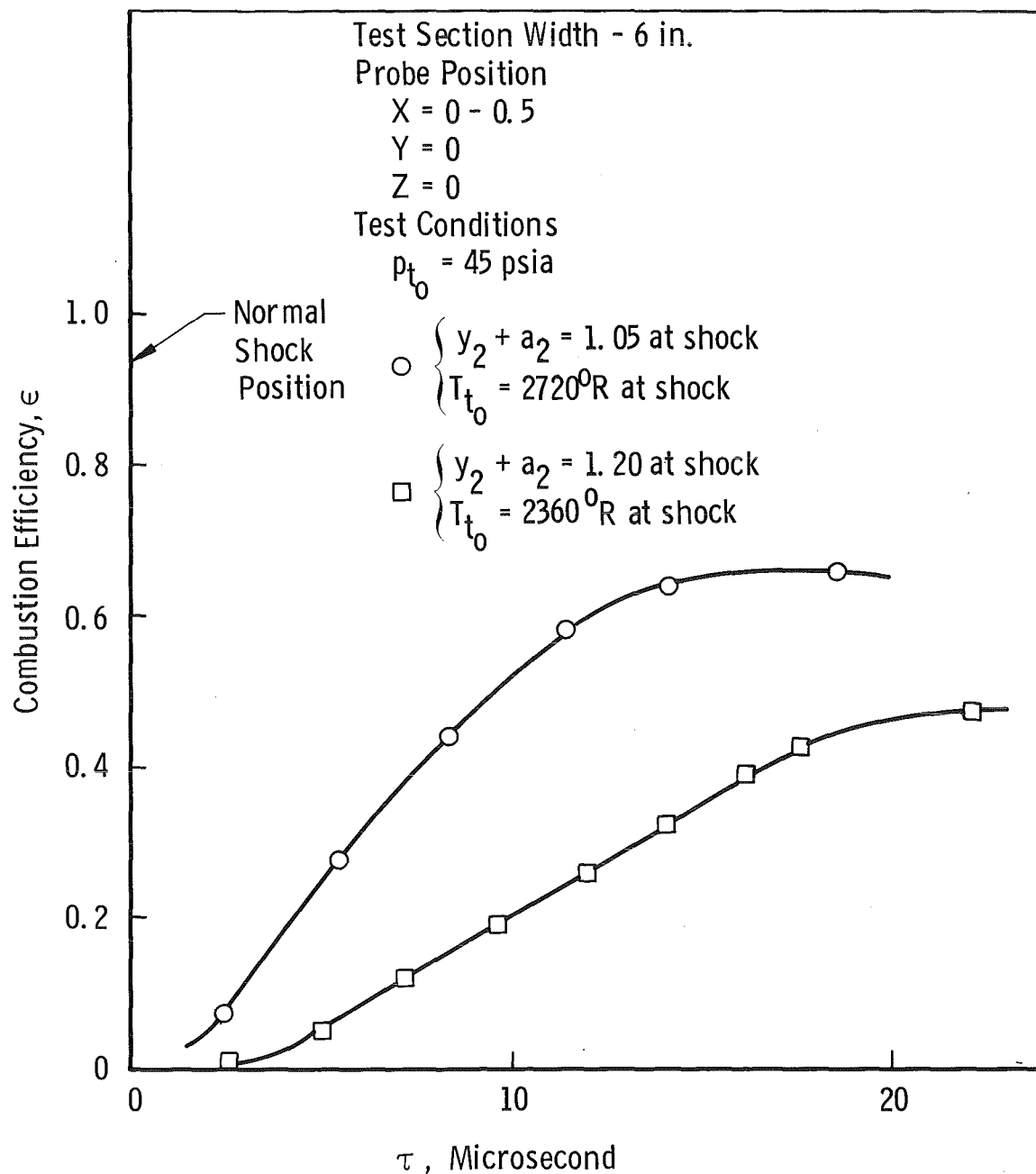


Fig. 18 Variation of Combustion Efficiency with Residue Time Aft of the Normal Shock

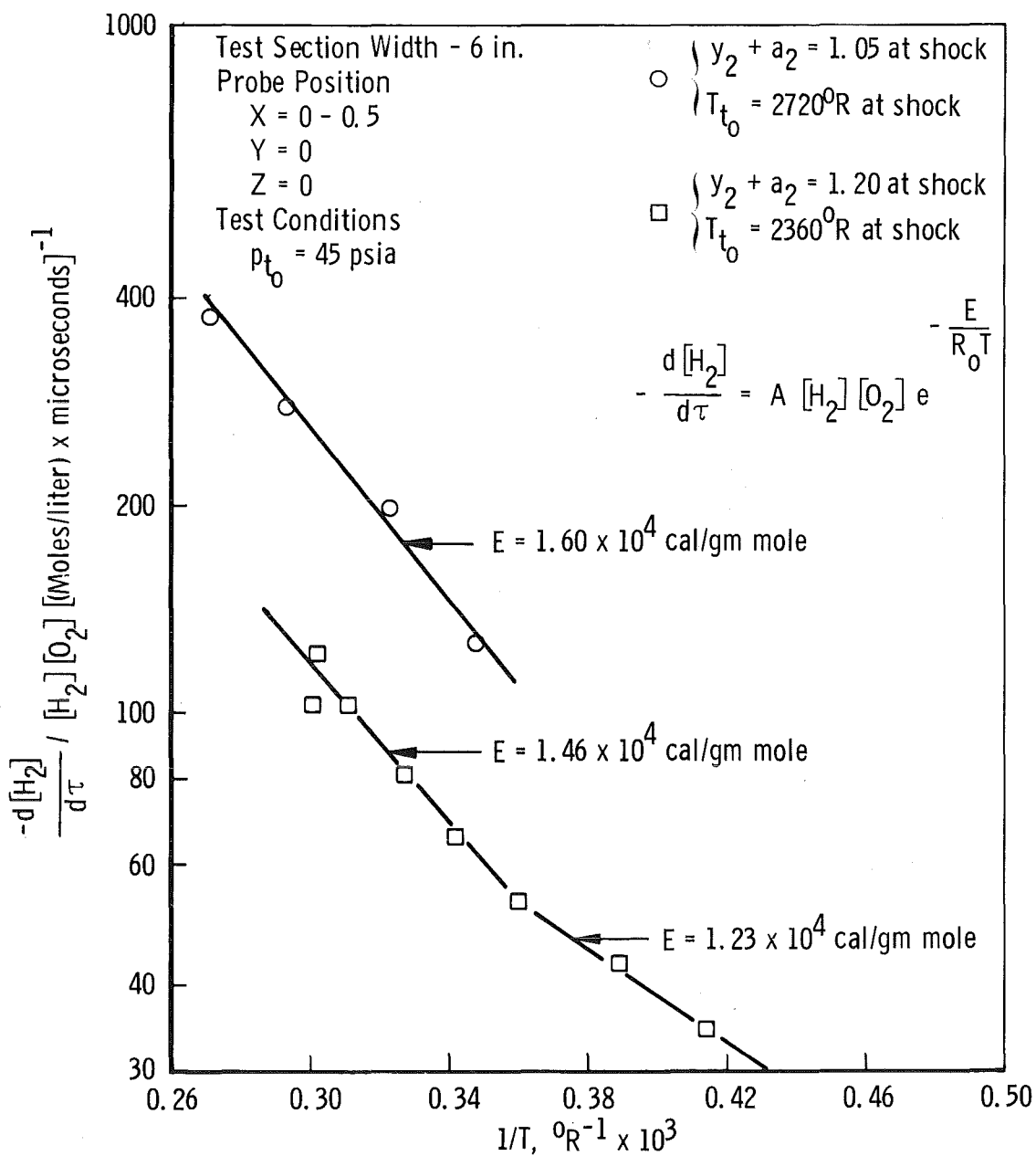


Fig. 19 Correlation of a Global Rate Equation for the Hydrogen-Oxygen Reaction



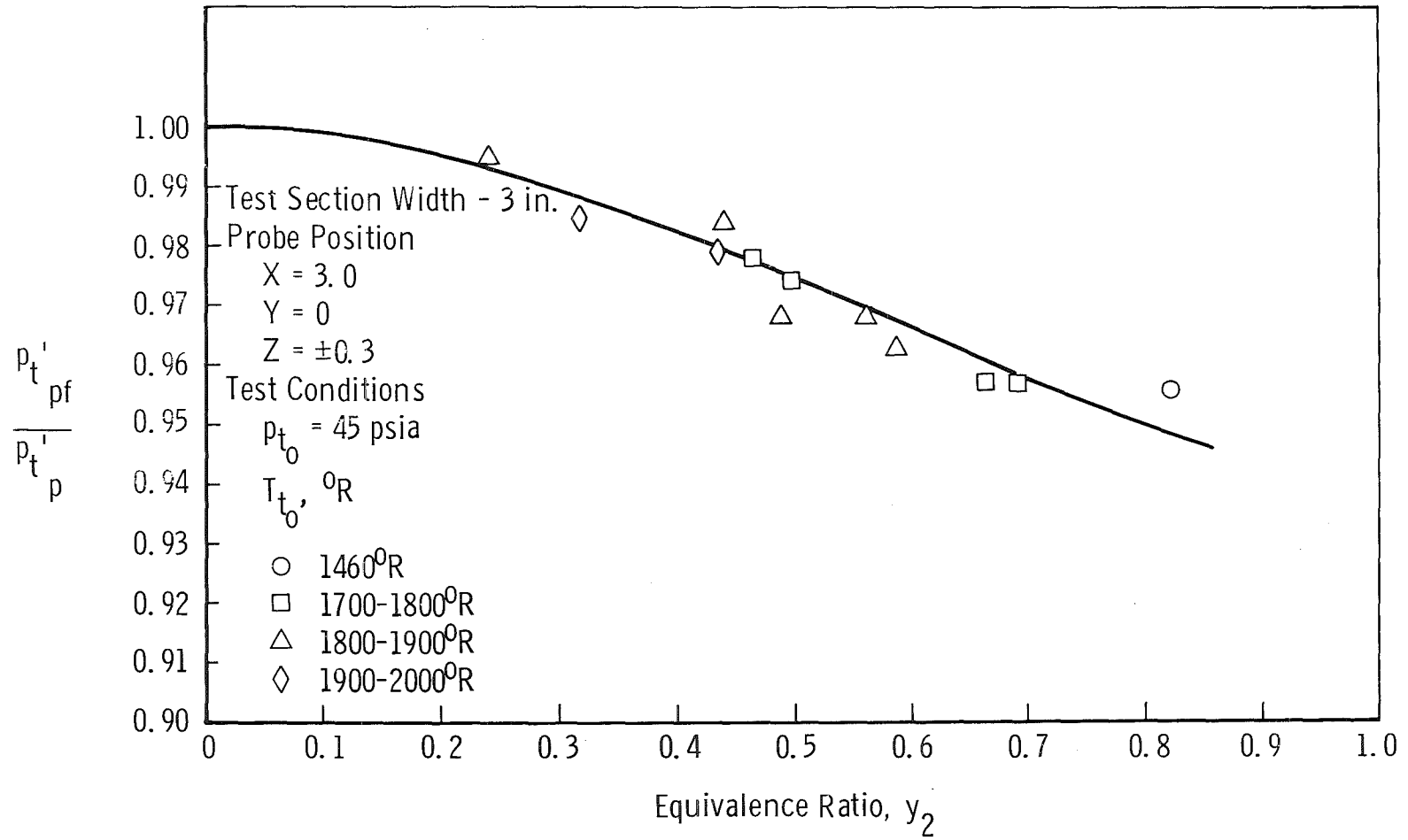


Fig. 20 Total Pressure Loss vs Fuel Concentration with Near-Zero Heat Release

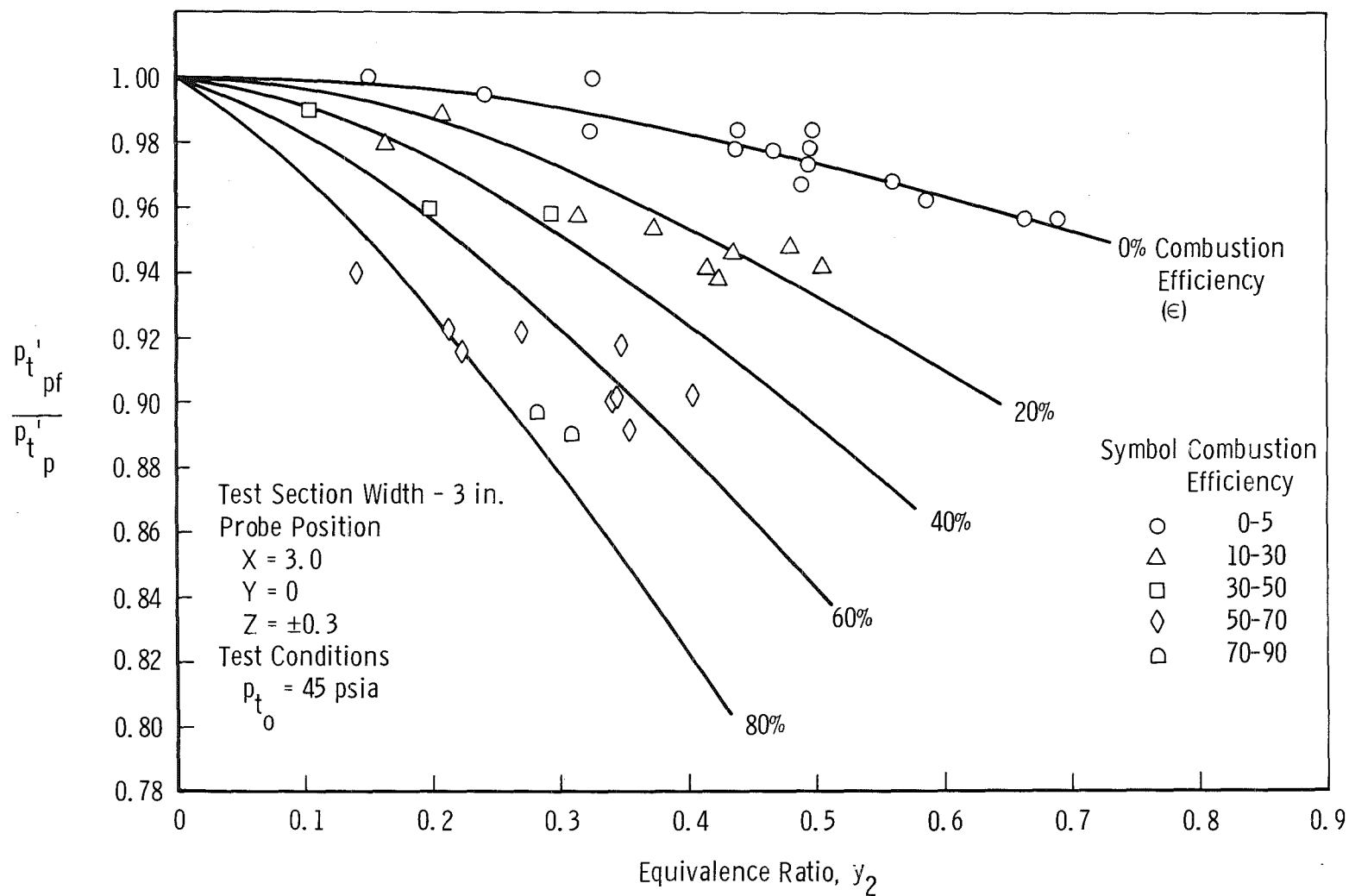


Fig. 21 Total Pressure Loss vs Fuel Concentration at Various Combustion Efficiency Values

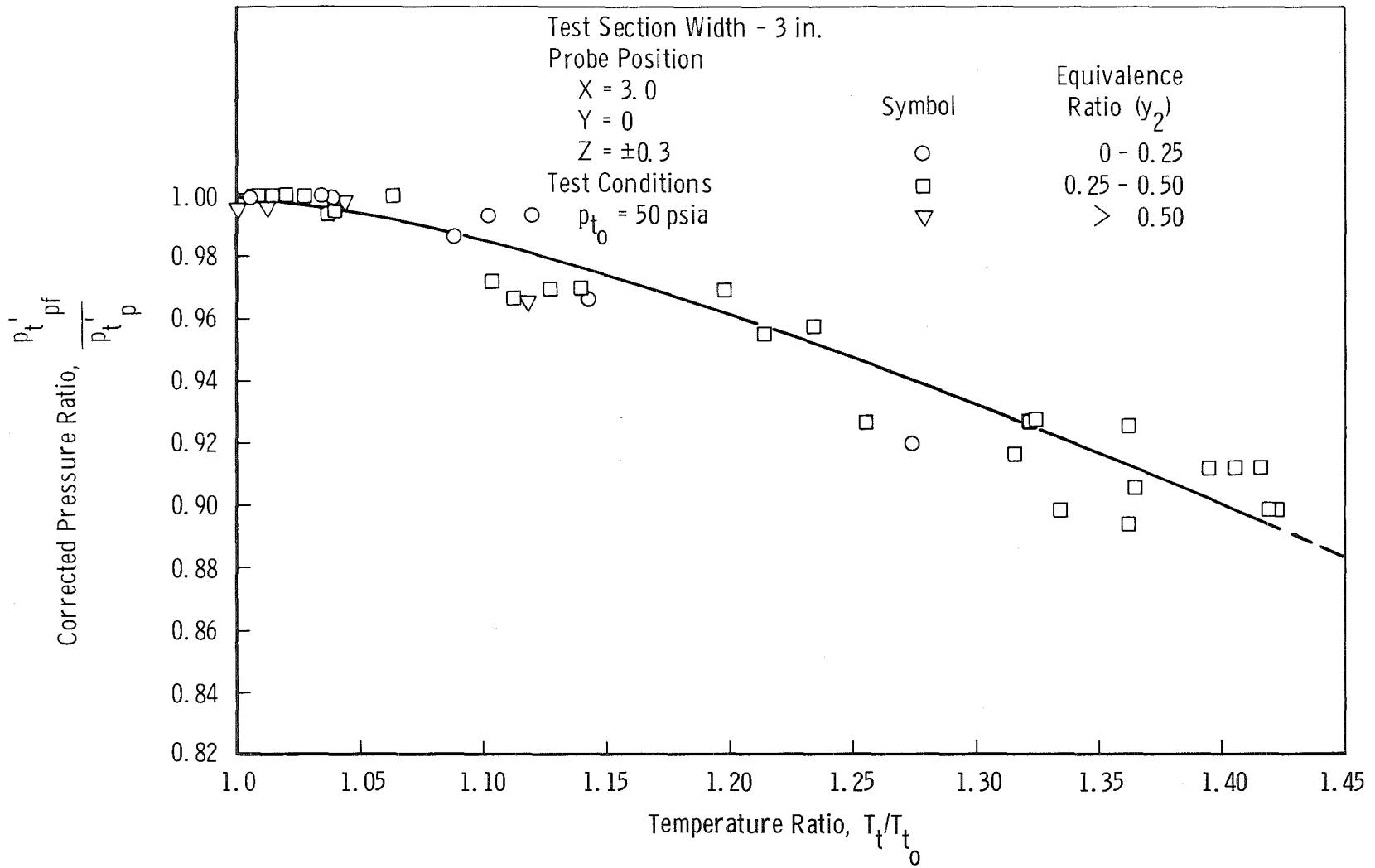


Fig. 22 Corrected Total Pressure Loss vs Temperature Ratio Three Inches Aft of the Normal Shock

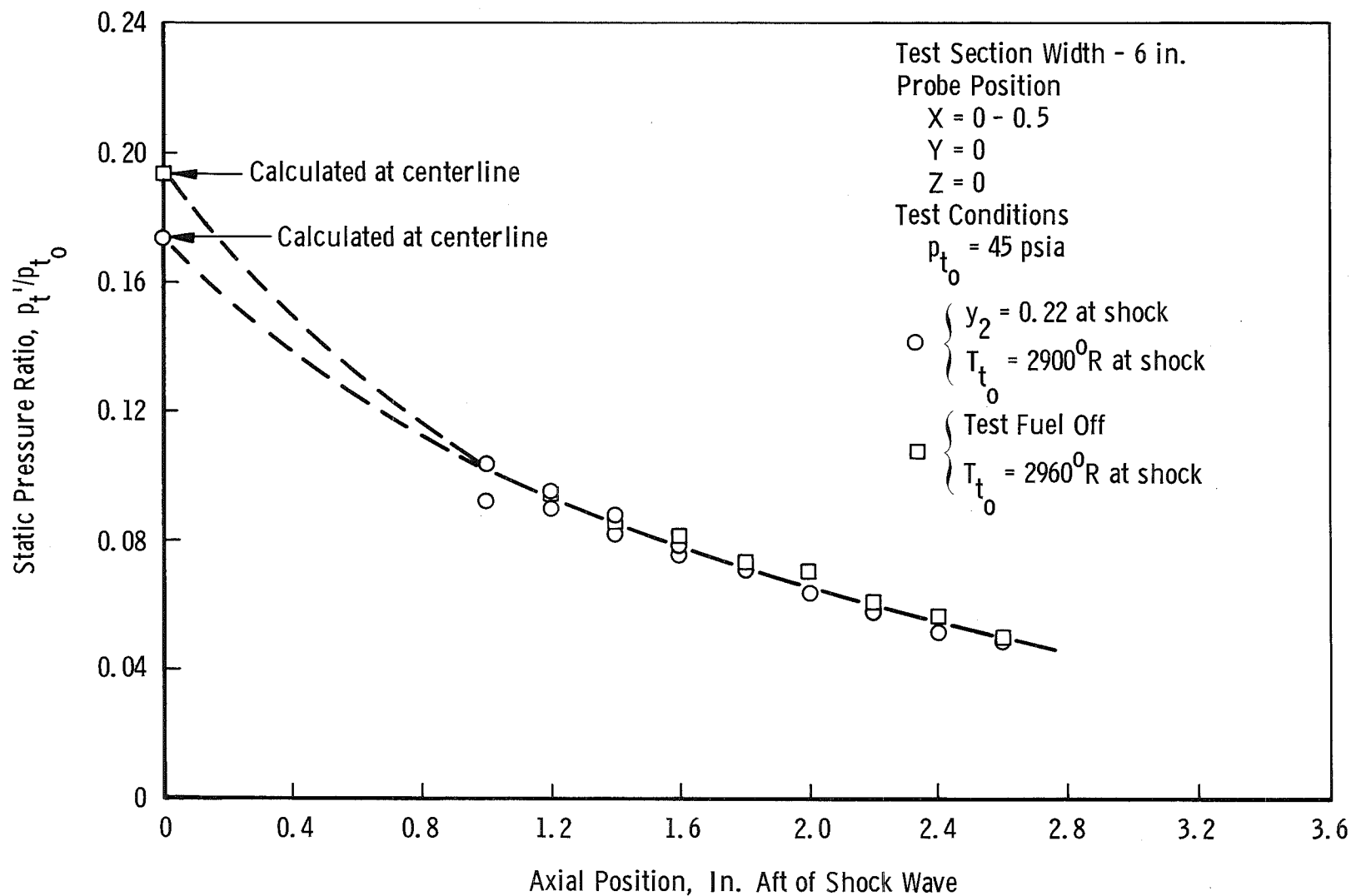
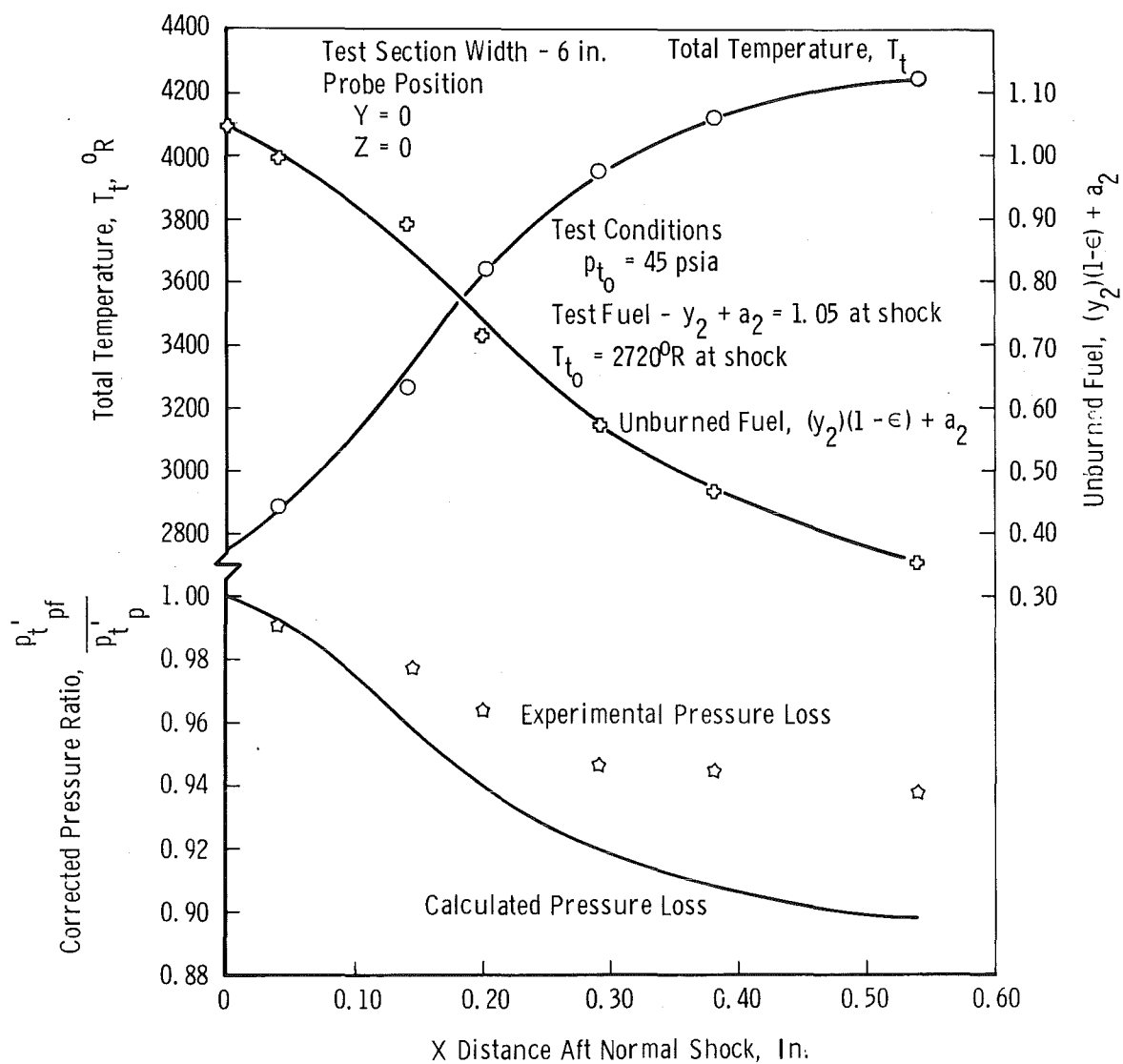
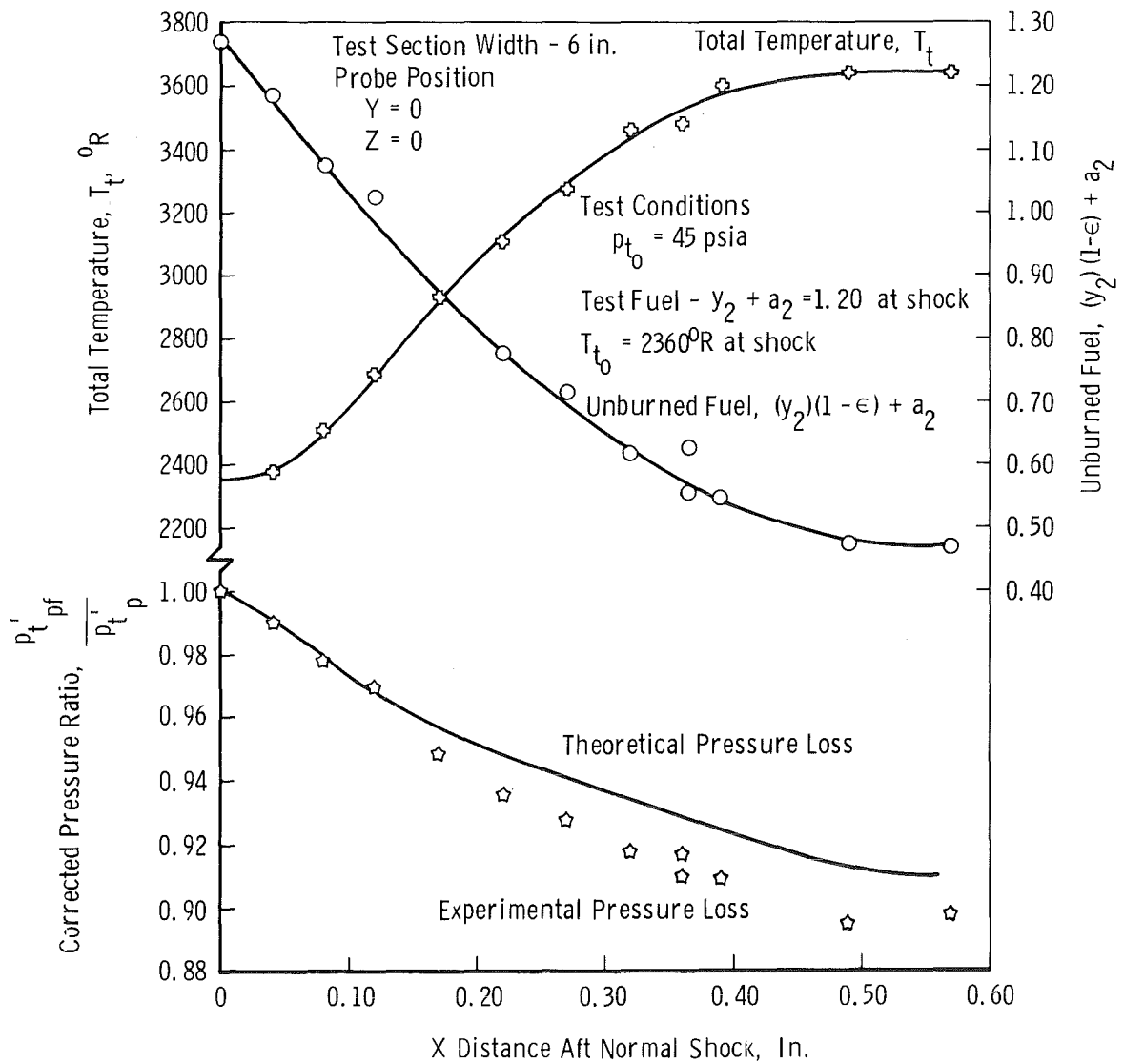


Fig. 23 Variation of Flow Parameters with Axial Distance Aft of Normal Shock Wave with Test Fuel



a.  $T_{t0}$  at shock  $2750^\circ\text{R}$

Fig. 24 Comparison of Calculated Pressure Loss with Experimental Pressure Loss for Heat Addition Aft of the Normal Shock



b.  $T_{t0}$  at shock  $2350^\circ\text{R}$

Fig. 24 Concluded

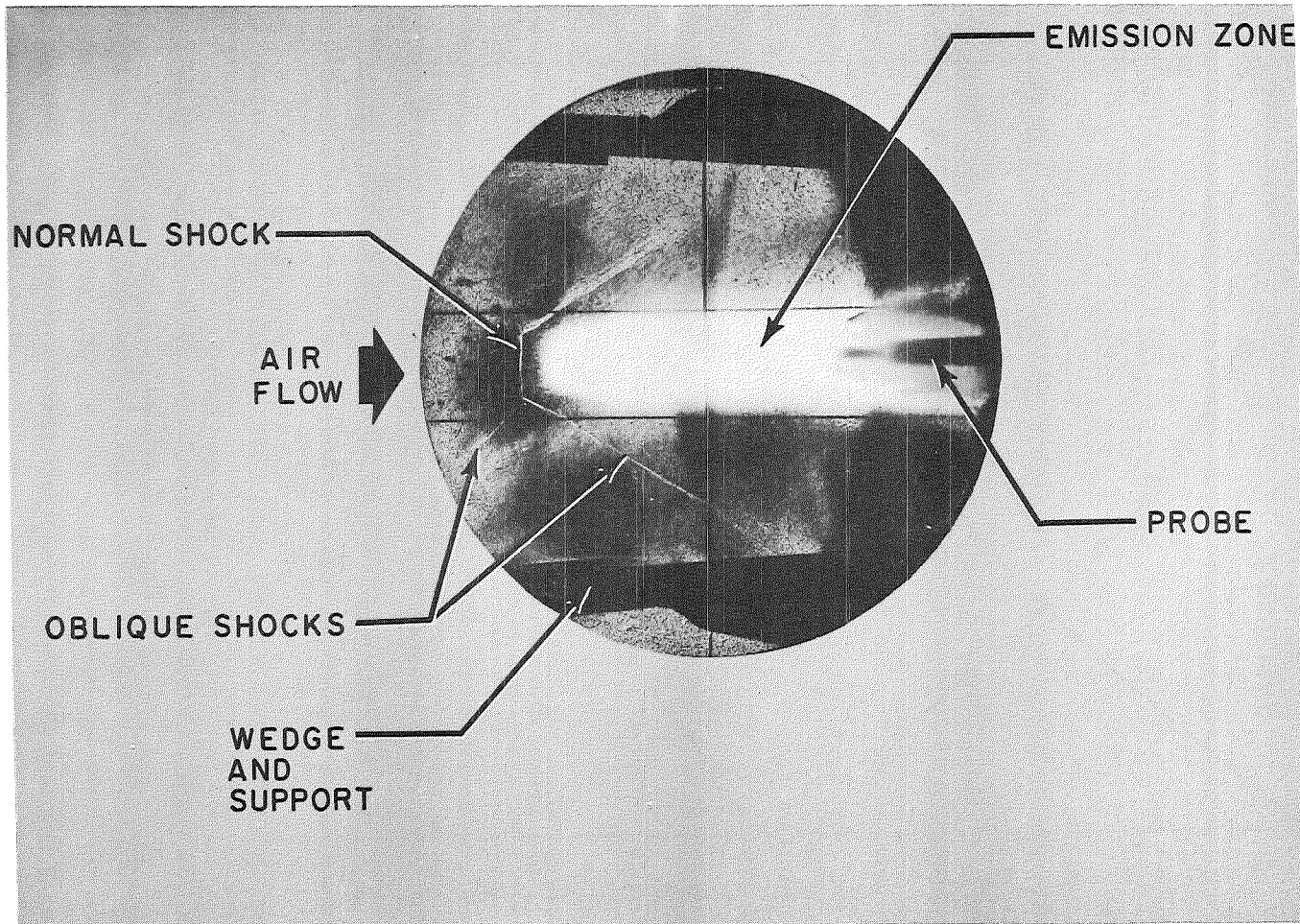


Fig. 25 Test Section Schlieren and Emission Photograph with Test Fuel On

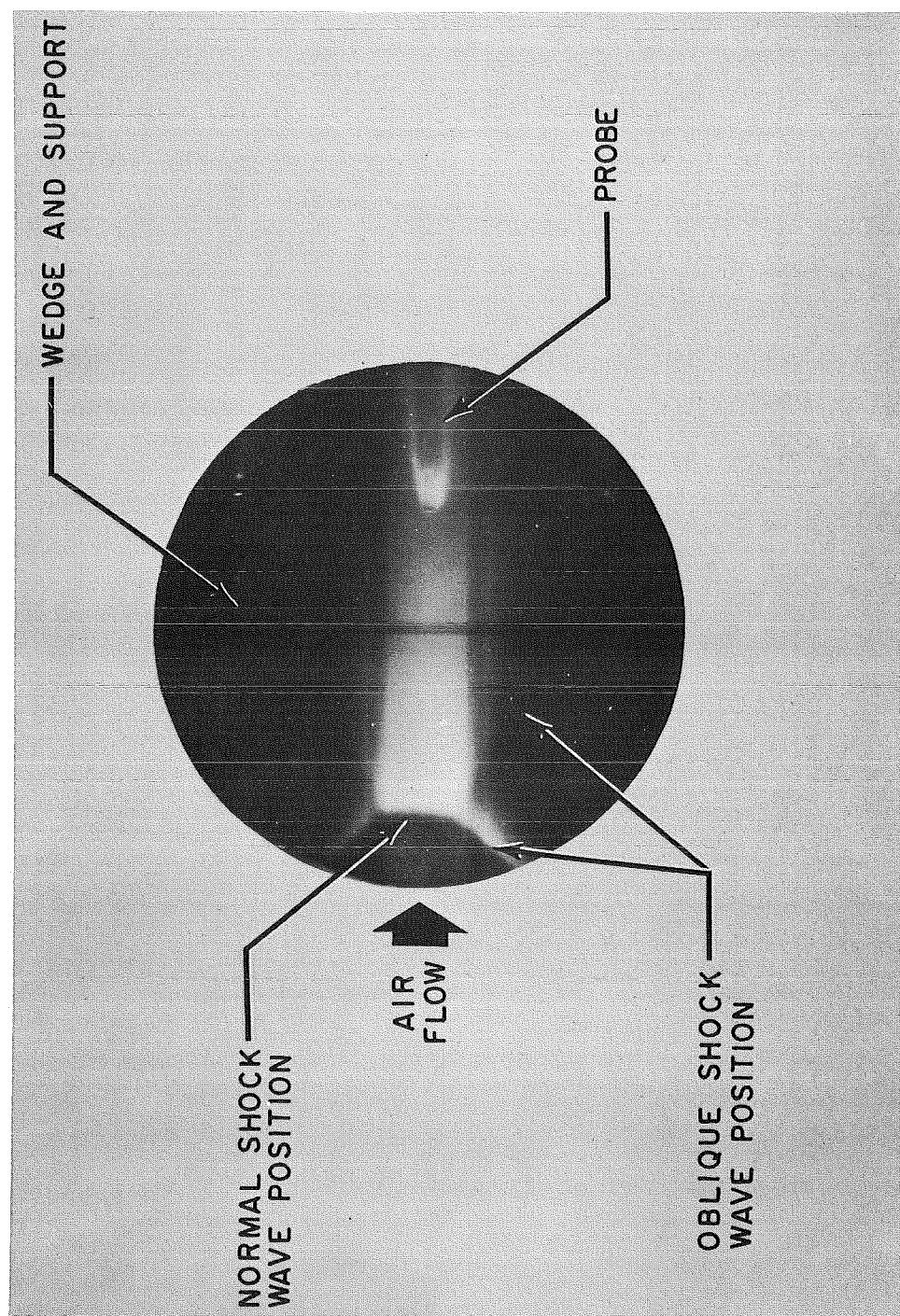


Fig. 26 Test Section Emission Photograph with Test Fuel Off



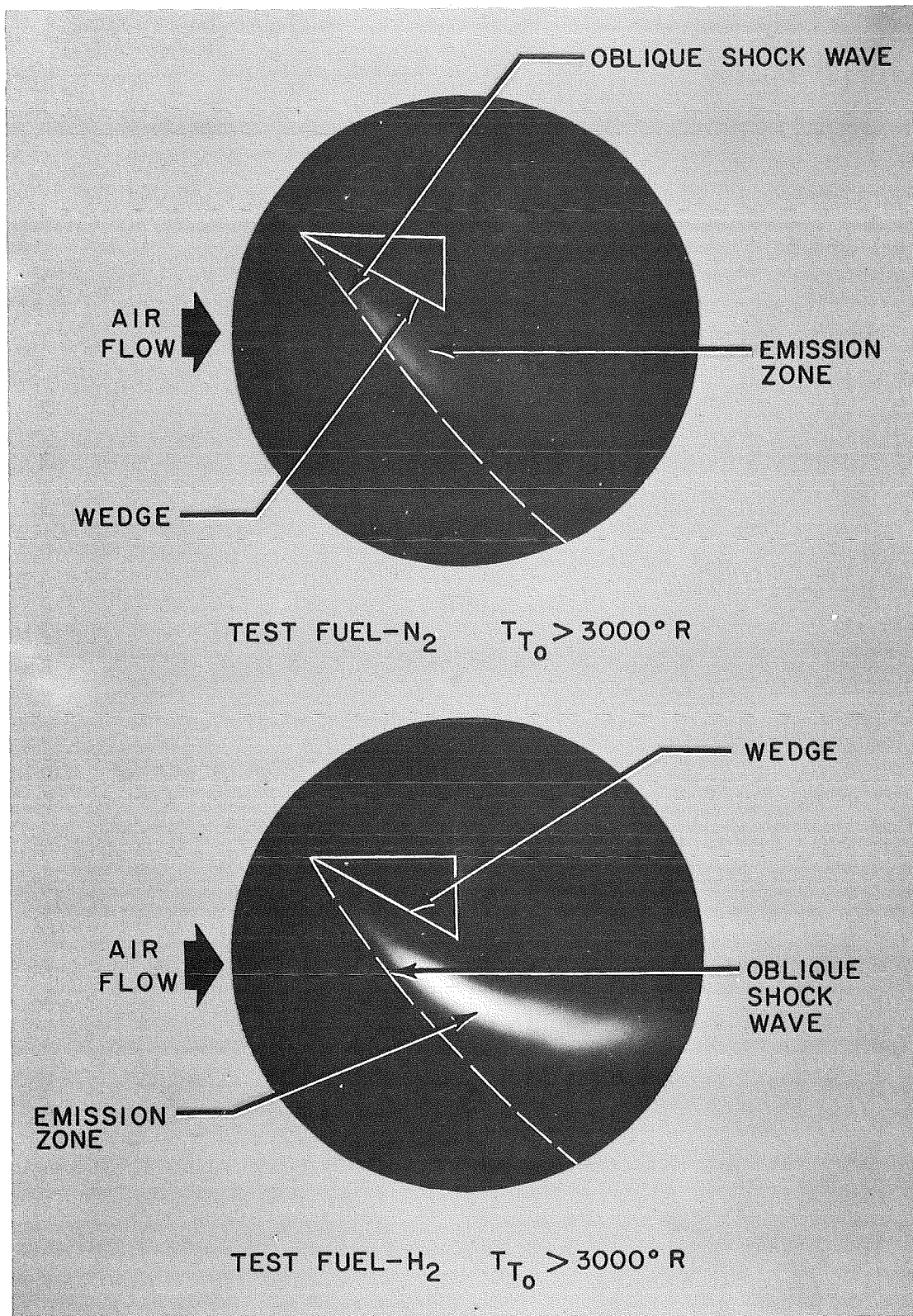


Fig. 27 Test Section Emission Photograph with Oblique Shock Wave